haematologica
Journal of the Ferrata Storti Foundation

Aberrant fucosylation of extracellular vesicles remodels the vascular microenvironment and promotes chemoresistance in myelodysplastic syndromes and acute myeloid leukemia

by Jingjing Feng, Kexin Wang, Junjie Gou, Yi Wang, Bowen Hu, Wei Wei, Junqi Ge, Yanli Feng, Shuang Feng, Eric Solary, Feng Guan and Xiang Li

Received: May 6, 2025
Accepted: February 26, 2026.

Citation: Jingjing Feng, Kexin Wang, Junjie Gou, Yi Wang, Bowen Hu, Wei Wei, Junqi Ge, Yanli Feng, Shuang Feng, Eric Solary, Feng Guan and Xiang Li. Aberrant fucosylation of extracellular vesicles remodels the vascular microenvironment and promotes chemoresistance in myelodysplastic syndromes and acute myeloid leukemia.
Haematologica. 2026 Mar 5. doi: 10.3324/haematol.2025.288146 [Epub ahead of print]

Aberrant fucosylation of extracellular vesicles remodels the vascular microenvironment and promotes chemoresistance in myelodysplastic syndromes and acute myeloid leukemia

Jingjing Feng[1,2#], Kexin Wang[1#], Junjie Gou[1,3 #], Yi Wang[4], Bowen Hu[1], Wei Wei[1], Junqi Ge[1], Yanli Feng[4], Shuang Feng[1], Eric Solary[2], Feng Guan[1], Xiang Li[1,5*]

1. Key Laboratory of Resource Biology and Biotechnology of Western China, Ministry of Education; Provincial Key Laboratory of Biotechnology, College of Life Sciences, Northwest University, Xi'an, China.
2. INSERM U1287, Université Paris-Saclay, Gustave Roussy Cancer Center, Villejuif, France.
3. Xi'an No. 1 Hospital, First Affiliated Hospital of Northwest University, School of Medicine, Xi'an, China.
4. Department of Hematology, Provincial People's Hospital, Xi'an, China.
5. Institute of Hematology, School of Medicine, Northwest University, Xi'an, China.

The authors have declared that no conflict of interest exists.

# Authors contributed equally.

*Correspondence to Xiang Li (e-mail: xiangli@nwu.edu.cn), Tel: +86-29-88303534, College of Life Science, Northwest University, 229 Taibai North Road, Xi'an, Shaanxi 710069, China

Funding

This study was supported by the National Science Foundation of China (No. 92478123, 82370147, 32371336), and Science Foundation for Distinguished Young Scholars of Shaanxi Province (No.2025JC-JCQN-061).

Acknowledgment

We appreciate Xinwen Yu for his assistance in drawing the conceptual model.

Authors' contributions

XL conceptualized the study and acquired funding. XL and JF designed the methodology. JF curated the data, conducted the formal analysis, and prepared the visualizations. JF, KW, JG, BH, WW, JG and SF carried out the investigation. YW and YF provided resources. XL oversaw project administration, while XL, ES, and FG supervised the study. JF wrote the original draft, and XL, ES, and FG contributed to reviewing and editing the manuscript in collaboration with JF. All authors have reviewed and approved the final version of the manuscript.

Competing interests

The authors declare that they have no competing interests.

Availability of data and materials

The datasets generated and analyzed during the current study are available from the corresponding author on reasonable request. Raw mass spectrometry data have been deposited in the GlycoPOST repository under accession GPST000674.

Abstract

Primary resistance to hypomethylating agents (HMAs) remains a major obstacle in the treatment of elderly patients with myelodysplastic syndromes (MDS) and acute myeloid leukemia (AML). An altered integrity of the vascular wall is suspected to contribute to this resistance, yet the underlying molecular mechanisms remain unclear. Here, we show that small extracellular vesicles (sEVs) derived from leukemic cells resistant to decitabine (DAC-R), a commonly used HMA, promote vascular permeability by downregulating tight junction proteins, including ZO-1, occludin, and claudin5, in endothelial cell monolayers. This disruption of vascular integrity may facilitate vascular leakage and leukemic cell dissemination. Mechanistically, DAC-R cells exhibit increased expression of the fucosyltransferase *FUT4*, driven by the transcription factor TWIST1, leading to enhanced biosynthesis of non-sialylated Lewis X (Le^X) structures. FUT4-mediated Le^X modification stabilizes intercellular adhesion molecule 3 (ICAM3) on sEVs, and the delivery of Le^X-modified ICAM3 to endothelial cells suppresses NF-κB signaling, impairing endothelial barrier function. Functionally, vascular remodeling driven by fucosylated sEVs promotes leukemic dissemination, suggesting that disruption of vascular homeostasis represents an additional layer of therapeutic resistance. These findings define a TWIST1–*FUT4*–Le^X–ICAM3 axis and highlight glycosylation as a critical mediator of vascular microenvironment remodeling in MDS/AML.

Keywords

Decitabine resistance, small extracellular vesicles (sEVs), FUT4, Lewis X, ICAM3,

Introduction

Primary resistance to hypomethylating agents (HMAs) such as 5-aza-2′-deoxycytidine (decitabine, DAC) represents a major obstacle to the treatment of elderly patients with myelodysplastic syndromes (MDS) and acute myeloid leukemia (AML). [1-3] Leukemic cells that are refractory to the epigenetic and cytotoxic effects of the drug rapidly expand, leading to death. These refractory cells modulate the bone marrow niche, establishing a protective microenvironment that further promotes their survival and expansion under therapeutic pressure.[4] One of their targets is the vascular endothelium in which alteration of endothelial cell functions increases vessel permeability.[5] Small extracellular vesicles (sEVs) have emerged as key mediators in this dialogue between leukemic cells and their microenvironment as they facilitate the transfer of diverse molecules from one cell type to another.[6, 7]

One of the features of sEVs that contribute to their biological effects is their glycosylation profile. This crucial post-translational modification affects the folding, trafficking, stability, and activity of multiple glycoproteins. Accordingly, cancer initiation and progression, angiogenesis, invasion, metastasis, and chemoresistance were all associated with abnormal expression of glycosyltransferase enzymes and characteristic glycosylation profiles. For example, therapeutic resistance of chronic myeloid leukemia cells was related to the downregulation of *ST3GAL4*, which encodes an enzyme of the β-galactoside-α2,3-sialyltransferase family,[8] while the resistance of AML cells to cytotoxic drugs was associated with overexpression of the

glycosyltransferase ALG9 in leukemic cells.[9] Importantly, the glycosylation profile of sEVs reflects that of donor cells and significantly influences their biological effects. For example, sEVs decorated with sialyl-Lewis ^{X} (sLe^{X}) facilitate bladder cancer metastasis by increasing vascular permeability,[10] whereas elevated bisecting GlcNAc modifications on sEVs derived from breast cancer cells mitigate their pro-metastatic potential.[11]

Our previous studies involved the interaction of the transcription factor TWIST1 with DNA methyltransferases 3 (DNMT3)[12] and the cellular transfer of miR-4755-5p in leukemic cell resistance to DAC.[13] The contribution of the glycosylation profile of leukemic cells and their sEVs to this resistance remained poorly explored. Here, we show that DAC-resistant MDS/AML cells demonstrate TWIST1-driven overexpression of the fucosyltransferase encoding gene *FUT4*, which promotes protein modifications with Lewis ^{X} (Le^{X}) structures. In turn, sEVs expressing Le^{X}-modified proteins such as ICAM-3 compromise endothelial integrity, increase vascular permeability and favor leukemic cell homing. These findings provide new insights into interactions between leukemic cells that are resistant to HMAs and surrounding vessels.

Methods

Patient samples

Plasma samples from healthy individuals (HD) and MDS/AML patients who are sensitive to DAC treatment (DAC-S group) or are refractory to DAC treatment (DAC-R-group) were collected from People's Hospital of Shaanxi Province (Tab. S1). Blood samples were collected into precoated EDTA tubes and immediately

centrifuged at room temperature for 15 min at 2000 g, and plasma samples were collected and frozen at − 80 ℃ until further use Written informed consent was obtained from all patients in accordance with the Declaration of Helsinki. The study was approved by the Medical Ethics Committee of Northwest University (approval number: 230306006, 6 March 2023).

In vivo mouse model

All mouse experiments were approved by the Animal Care and Use Committee of Northwest University (approval number: NWU-AWC-20231202M, 2 December 2023). Briefly, 6~8-week-old B-NSG mice (NOD-Prkdcscid*IL2rg*tm1/Bcgen, NSG; Biocytogen Pharmaceuticals, Beijing, China) were irradiated with 3Gy., followed by tail vein injection of 10^7 KG1a or KG1a-DAC cells. After 16 h, mononuclear cells in blood, bone marrow, and spleen stained with antibody against human CD45 (#561865, BD Biosciences; Franklin Lakes, NJ, USA) and the percentages of human CD45+ cells were analyzed by FACS.

For sEVs pre-conditioned mice, sEVs (50 μg in 100 μL PBS) from HD, KG1a, KG1a-FUT4, KG1a-DAC, KG1a-DAC-shFUT4 were i.v. injected into NSG mice three times per week for two weeks, and then irradiated with 3Gy., followed by i.v. injected of 10^7 KG1a cells. The percentages of human CD45+ cells in blood, bone marrow, and spleen were analyzed by FACS.

Statistical analysis

Each experiment was performed at least three times. Prism 8.0 Statistical Software program (GraphPad Software; La Jolla, CA, USA) was used for statistical

analysis. Intergroup means were compared using Student's *t*-test, and multiple group comparisons were evaluated by one way ANOVA with Bonferroni's post hoc test. Data are presented as mean ± SEM. Differences at $p<0.05$ were considered statistically significant. *, $p < 0.05$; **, $p < 0.01$; ***, $p < 0.001$.

Results

Decitabine (DAC) resistant leukemic cells increase endothelial permeability

We first performed a xenotransplantation experiment in which KG1a parental cells and DAC-resistant (KG1a-DAC) cells were injected intravenously to irradiated B-NSG mice. Sixteen hours after injection, the fraction of KG1a-DAC cells was lower in the peripheral blood while being higher in the bone marrow and the spleen when compared to KG1a parental cells (**Fig. 1A**). One of the features associated with chemoresistance of MDS/AML is an increased vascular permeability that may promote leukemic cell homing. [14, 15] Accordingly, in co-culture experiments performed in a transwell device, KG1a-DAC cells increased the permeability of HUVEC monolayers (**Fig. S1A**). In accordance with the role of cell-cell junctions in endothelium permeability,[16] immunoblot analyses detected a decreased expression of ZO-1, occludin and claudin5 in HUVECs co-cultured with KG1a-DAC compared to KG1a cells (**Fig. S1B**).

Interestingly, a similar decrease in the expression of ZO-1, occludin and claudin5 was detected in HUVECs co-cultured for 48 hours with plasma collected from MDS/AML patients refractory to DAC (DAC-R), as compared to plasma collected from patients sensitive to the drug (DAC-S) and healthy donor (HD) plasma (**Fig. 1B**).

Plasma collected from MDS/AML patients who responded to DAC was observed to increase the trans-endothelial migration of GFP-labeled KG1a cells (**Fig. 1C**), the permeability of HUVEC monolayers to rhodamine (**Fig. 1D**) and the formation of tubes (**Fig. 1E, S1C**). All these effects were amplified when plasma was collected from MDS/AML patients who did not respond to DAC (**Fig. 1C-E, S1C**). Similar results were observed when HUVEC monolayers were treated with conditioned media (CM) collected after 48 hours of culture of KG1a-DAC, compared to KG1a-CM collected in the same conditions (**Fig. S1D-G**).

Small extracellular vesicles released by myelodysplastic syndromes and acute myeloid leukemia (MDS/AML) cells impair the endothelial barrier

Recognizing the pivotal role of sEVs in facilitating metastasis by compromising vascular integrity,[16, 17] we performed ultracentrifugation to sort sEVs from KG1a and KG1a-DAC CM. These sEVs exhibited a typical spherical shape (**Fig. S2A&B**), a consistent size distribution peaking at approximately 100 nm (**Fig. S2C&D**), and a strong expression of canonical sEVs markers such as CD63, Alix, and Tsg101 (**Fig. S2E&F**).

Treatment of HUVEC monolayers with sEVs derived from KG1a-DAC-CM resulted in a significant decrease in ZO-1, occludin, and claudin5 expression (**Fig. 2A**), increased permeability (**Fig. 2B**), and enhanced tube formation (**Fig. 2C**) compared to sEVs collected from KG1a-CM. Consistent with these observations, HUVEC monolayers exposed to plasma sEVs collected from DAC-R patients exhibited a significant reduction in ZO-1, occludin, and claudin5 (**Fig. 2D**), increased permeability

(**Fig. 2E**), and enhanced tube formation (**Fig. 2F, S2G**) when compared to those treated with plasma sEVs collected from HD and DAC-S patients.

Small extracellular vesicles (sEVs) released by decitabine (DAC)-refractory leukemic cells demonstrate aberrant fucosylation

We previously reported the aberrant glycosylation pattern of sEVs released by resistant leukemic cells.[18] Because patient plasma contains a mixture of vesicular and non-vesicular glycoconjugates, we next analyzed plasma N-glycan composition by MALDI-TOF/TOF-MS (**Fig. S3A-C, Tab. S4**) to obtain an overview of systemic glycosylation changes among HD, DAC-S, and DAC-R patients. This global analysis suggested increased fucosylation in the plasma collected from DAC-R patients (**Fig. S4A-C**). In parallel, we isolated sEVs from the KG1a and KG1a-DAC cells, respectively, and performed MALDI-TOF/TOF-MS–based N-glycomic profiling. Consistent with the plasma analysis, sEVs derived from KG1a-DAC exhibited an overall increase in fucosylated N-glycans (**Fig. S4D&E, Tab. S4**).

And then we performed lectin blot assays using *Lens Culinaris* Agglutinin (LCA) and *Aleuria Aurantia* Lectin (AAL), which specifically recognize core α1,6-fucose and terminal α1,3/α1,4/α1,6-fucose, respectively. Both LCA and AAL signals were increased in sEVs from DAC-R patients compared with DAC-S, with AAL signal being the highest signal (**Fig. 3A**). Consistently, the Lectin-based ELISA assay demonstrated increased AAL plasma levels (**Fig. S4F**), which were also detected in sEVs (**Fig. 3B**) when collected from the plasma of DAC-R compared to DAC-S patients and from HD. In line with patient findings, AAL reactivity was strongly

enhanced in KG1a-DAC cells and their sEVs (**Fig. 3C&D**).

Fucosyltransferase (FUT) genes encode enzymes that transfer an L-fucose sugar from a GDP-fucose (guanosine diphosphate-fucose) donor substrate to an acceptor substrate. RT-qPCR analyses detected an increased expression of several genes of the *FUT* family, including *FUT3*, *FUT4*, *FUT6*, *FUT7* and *FUT8*, in KG1a-DAC cells compared to KG1a parental cells, contrasting with a significant decrease in the expression of *FUT5* and *FUT9* genes (**Fig. 3E**). Among these genes, we selected *FUT4* gene whose expression was the highest detected in resistant cells (**Fig. S4G**).

Lewis^X enhances leukemic cell homing and vascular permeability

FUT4 encodes a fucosyltransferase that primarily catalyzes the biosynthesis of non-sialylated Lewis^X (Le^X, also known as CD15) (**Fig. 4A**). Le^X is expressed on a variety of glycolipids and glycoproteins on the cell surface of neutrophils, monocytes, eosinophils and non-hematopoietic tissues, and in our system was abolished by PNGase F treatment (**Fig. S4H**).[19] Le^X levels were markedly increased in sEVs isolated from DAC-R patient plasma compared with DAC-S and HD samples (**Fig. S4I**). Compared to KG1a parental cells, Le^X expression was increased at the surface of KG1a-DAC (**Fig. 4B, S4J**) as well as in their derived sEVs (**Fig. 4B**). We overexpressed *FUT4* gene in KG1a cells (designated as KG1a-FUT4), which resulted in a significant increase in Le^X levels (**Fig. 4C**), A similar trend was also observed in the corresponding sEVs (**Fig. 4C**). Treatment of HUVEC monolayers with sEVs or CM from KG1a-FUT4 cells reduced ZO-1, occludin, and claudin5 expression (**Fig. 4D,**

S5A), along with increased permeability (**Fig.4E, S5B&C**).

In contrast, knockdown of *FUT4* in KG1a-DAC cells (KG1a-DAC-shFUT4) significantly decreased Le^X levels in both cells and derived sEVs (**Fig. S5E&F**). Treatment of HUVEC monolayers with sEVs or CM from KG1a-DAC-shFUT4 cells upregulated ZO-1, occludin, and claudin5 expression (**Fig. S5G&H**), and decreased permeability (**Fig. S5I&J**). Furthermore, sEVs or CM from KG1a-FUT4 cells enhanced tube formation (**Fig. 4F&S5D**), while KG1a-DAC-shFUT4 sEVs or CM reduced it (**Fig. S5K&L**). Furthermore, treatment of HUVECs with OptiPrep-purified sEVs from KG1a-DAC or KG1a-FUT4 cells reduced ZO-1, occludin, and claudin5 expression, while KG1a-DAC-shFUT4 sEVs restored them (**Fig. S5M**), confirming the sEVs-specific endothelial effects.

Next, we investigated whether Le^X promotes leukemic cell homing by enhancing vascular permeability. NSG mice were preconditioned with sEVs from HD, KG1a, KG1a-DAC, KG1a-FUT4, or KG1a-DAC-shFUT4 cells, followed by intravenous injection of KG1a cells (**Fig. 4G, S5N**). Mice pretreated with HD-sEVs showed no significant enhancement of leukemic cell homing, as indicated by higher levels of circulating $hCD45^+$ cells and fewer cells in bone marrow and spleen compared with the KG1a-sEVs group (**Fig. S5N**). In contrast, KG1a-DAC-sEVs and KG1a-FUT4-sEVs significantly increased KG1a cell homing to the bone marrow and spleen, accompanied by fewer circulating cells in peripheral blood. Conversely, KG1a-DAC-shFUT4-sEVs reduced KG1a cell homing to the BM and spleen, with more cells being retained in the peripheral blood (**Fig. 4G**).

Enhanced vascular permeability involves TWIST1-driven *Fucosyltransferase 4 (FUT4)* gene expression

Since we previously associated MDS/AML cell resistance to DAC with an elevated expression of TWIST1,[12] a basic helix-loop-helix transcription factor, we explored TWIST1 impact on *FUT4* gene expression and Le^X level. TWIST1 was overexpressed in KG1a (KG1a-TWIST1) (**Fig. 5A**, **S6A**) and was stably knocked down in SKM1(SKM1-shTWIST1) (**Fig. S6B&C**), an MDS cell line that spontaneously expresses high levels of TWIST1. When HUVEC monolayer was incubated with CM from KG1a-TWIST1 cells, we observed a decrease in ZO-1, occludin, and claudin5 expression (**Fig. 5B**), an increased permeability (**Fig. 5C**) and an enhanced tube formation (**Fig. 5D**). In contrast, CM from SKM1-shTWIST1 cells increased ZO-1, occludin, and claudin5 expression (**Fig. S6D**), decreased permeability (**Fig. S6E&F**), and reduced tube formation (**Fig. S6G**).

TWIST1 binds preferentially to E-box DNA promoter sequences (-CANNTG-) in target gene promoters.[20, 21] Analysis of the *FUT4* promoter (-2.0 kb) identified seven E-box motifs (**Fig. S6H**). ChIP assays revealed a strong binding of TWIST1 to motifs 1, 2, and 7 while binding to motifs 3, 4, 5, and 6 was weak (**Fig. 5E**). A luciferase reporter assay confirmed that TWIST1 overexpression strongly enhanced FUT4-WT promoter activity, whereas mutation of the first E-box motif (FUT4-M1) markedly reduced TWIST1-mediated transactivation (**Fig. 5F, S6I**). These findings demonstrate that TWIST1 enhances *FUT4* gene transcription by binding to the first E-box motif of its promoter.

Intercellular adhesion molecule 3 (ICAM3) identified as key Lewis^X-modified protein

Using quantitative proteomic analysis, we identified differentially expressed proteins in KG1a, KG1a-FUT4, KG1a-DAC, and KG1a-DAC-shFUT4 cells. A total of 77 proteins were differentially expressed (fold change >1.5 or <0.67; $p < 0.05$) across these groups (**Fig. 6A**). Notably, intercellular adhesion molecule 3 (ICAM3), a key adhesion molecule involved in promoting angiogenesis, was significantly increased in KG1a-DAC and KG1a-FUT4 while being decreased in KG1a-DAC-shFUT4 (**Fig. 6B**). Immunoprecipitation (IP) assay confirmed enhanced Le^X modification on ICAM3 in KG1a-DAC and KG1a-FUT4 cells, whereas this modification was reduced in KG1a-DAC-shFUT4 cells (**Fig. 6C**). Consistently, the presence of ICAM3 on sEVs was clearly revealed by density gradient fractionation (**Fig. S7A**). Additionally, ICAM3 and Le^X expression was upregulated in sEVs from KG1a-DAC and KG1a-FUT4 cells, but downregulated in sEVs from KG1a-DAC-shFUT4 (**Fig. S7B&C**). Inhibiting protein synthesis with cycloheximide (CHX) revealed slower degradation of ICAM3 in KG1a-FUT4 cells compared to KG1a cells (**Fig. S7D**). Further study demonstrated that Le^X modification stabilizes ICAM3 by inhibiting its degradation via the lysosomal pathway (**Fig. S7E**).

Lewis^X -modified intercellular adhesion molecule 3 (ICAM3) enhances vascular permeability via NF-kB signaling

Since the transcription factor NF-kB regulates the expression of genes that modulate the vascular barrier,[22] we treated HUVEC monolayers cells with the NF-kB

signaling inhibitor BAY-11-7082, which decreased the expression of ZO1, occludin, and claudin5 (**Fig. S7F&G**). Conversely, stimulation of HUVEC monolayers with phorbol 12-myristate 13-acetate (PMA), an activator of NF-κB signaling, led to increased phosphorylation of P65 and IκBα and a time-dependent increase in ZO-1, occludin, and claudin5 expression (**Fig. S7H&I**). Furthermore, treatment of HUVEC monolayers with sEVs from KG1a-DAC or KG1a-FUT4 reduced phosphorylation of p65 (p-p65) and IκBα (p-IκBα) levels in these cells, while sEVs from KG1a-DAC-shFUT4 enhanced NF-kB activation (**Fig. S7J**). In HUVEC monolayers, treatment with sEVs from KG1a-DAC or KG1a-FUT4 significantly downregulated p-p65 and p-IκBα signaling and reduced the expression of ZO-1, occludin, and claudin5, while these effects were partly reversed by anti-human ICAM3 antibody treatment (**Fig. 6D, S8A**). These sEVs also increased permeability and tube formation and these effects were mitigated by α-ICAM3 treatment (**Fig. 6E&F, S8B-D**). Conversely, sEVs from KG1a-DAC-shFUT4 enhanced p-p65 and p-IκBα signaling, increased ZO-1, occludin, and claudin5 expression, and reduced permeability and tube formation in HUVECs. These effects were partly reversed by recombinant ICAM3 protein (rICAM3) (**Fig. S8E-H**). Finally, stable overexpression of *ICAM3* gene in HUVECs (HUVEC-ICAM3) led to reduced phosphorylation of p65 and IκBα, accompanied by decreased expression of ZO-1, occludin, and claudin5 (**Fig. S8I&J**), which was associated with an increased permeability of HUVEC monolayer (**Fig. S8K&L**) and an enhanced tube formation (**Fig. S8M**).

Discussion

Primary resistance of leukemic cells to HMAs, which is observed in ~50% of elderly patients with MDS or AML, remains a therapeutic challenge. The present study deciphers a pathway by which leukemic cells modulate their glycosylation profile and release sEVs that alter surrounding endothelial cell functions, leading to the disruption on vascular wall integrity with increased permeability and enhanced leukemic cell homing. Such a toxic interaction between leukemic cells and their microenvironment may contribute to therapeutic resistance.

The blood vessel endothelium integrity serves as a barrier that regulates hematopoietic cell migration into tissues.[23] Leukemic cells actively remodel their microenvironment by disrupting vascular integrity, thereby facilitating their homing to tissues and promoting their survival. [5] Recent studies have highlighted the role of leukemic cell-derived sEVs in mediating interaction between leukemic cells and their microenvironment, especially in the bone marrow niche.[24] sEVs from drug resistant malignant cells were shown also to generate pre-metastatic niches into distant tissues by promoting vascular development and permeability to facilitate tumor cell dissemination.[25, 26] Examples include sEVs generated by glioma stem cells that promote angiogenesis through activating the VEGF/VEGFR2 signaling pathway,[27] and cancer cell-derived sEVs that enhance tumor vascularization and trigger stroma remodeling through promoting CXCL8 secretion by mesenchymal stem cells.[28] We demonstrated recently that extracellular vesicles released from KG1a-DAC promote DAC-resistant through miR-4755-5p that reduces the expression of cyclin-dependent kinase inhibitor 2B (CDKN2B) in KG1a cells.[13] In the present study, we show that

sEVs released by DAC resistant leukemic cells, which exhibit elevated homing ability in a xenotransplantation mouse model, downregulate tight junction-associated proteins to increase vascular permeability.

We have shown previously that glycosylation modifications detected on leukemic cell derived sEVs contribute to reshaping their microenvironment.[18] Our glycomic analyses identify a significant upregulation of terminal fucosylation in DAC-R patients. More precisely, we found elevated levels of Le^X in sEVs collected from DAC-R plasma, highlighting the potential role of FUT4-driven fucosylation in therapy resistance. Such an increased FUT4-driven fucosylation was previously detected in AML stem cells,[29] and in metastatic colorectal cancer cells.[30]

Upstream of *FUT4* gene up-regulation, we identify TWIST1, an oncogenic transcription factor whose increased expression was depicted in chronic myeloid leukemia cells and involved in their resistance to the tyrosine kinase inhibitor imatinib.[31] TWIST1 expression was also detected in some MDS/AML cell lines and its overexpression was related to leukemogenesis and drug resistance, including resistance to DAC.[32] The present study identifies one of the seven E-box depicted within *FUT4* gene promoter as the primary binding site for TWIST1.

Downstream of FUT4 overpression, our quantitative proteomic analysis identifies ICAM3 as a Le^X-modified protein in DAC-resistant leukemic cells. Immunoprecipitation (IP) confirmed Le^X modification on ICAM3 in KG1a-DAC and KG1a-FUT4 cells while this modification was decreased in KG1a-DAC-shFUT4. Mechanistically, Le^X modification could stabilize ICAM3 by preventing its lysosomal

degradation. ICAM3 was shown to play a role in inflammatory signaling, cancer cell stemness and vascular permeability.[33, 34] Increased ICAM3 delivery through leukemic cell-derived sEVs to endothelial cells may inhibit NF-κB signaling, thereby disrupting vascular permeability,[22] thereby promoting MDS/AML cell tissue migration (**Fig. 7**). In line with this, our results show that FUT4-high sEVs suppress NF-κB activation by lowering p65 and IκBα phosphorylation in HUVECs, consequently downregulating tight junction proteins ZO-1 and occludin and compromising endothelial barrier integrity.

Together, this work deciphers a mechanism by which MDS/AML cells that are refractory to DAC release extracellular vesicles expressing modified proteins that reshape their microenvironment by increasing vascular permeability and leukemic cell migration into tissues. If this reshaped microenvironment affords stimulatory signaling that further enhance leukemic cell resistance to DAC and other anti-leukemic drugs, disruption of this stimulatory signaling may improve their therapeutic efficacy. In this context, therapeutic strategies aimed at inhibiting FUT4 activity or blocking Le^X modification of ICAM3 may serve as promising adjuncts to HMAs, with the potential to normalize endothelial barrier function, limit leukemic cell homing, and reduce microenvironmental protection.

Reference

1. Šimoničová K, Janotka Ľ, Kavcová H, Sulová Z, Breier A, Messingerova L. Different mechanisms of drug resistance to hypomethylating agents in the treatment of myelodysplastic syndromes and acute myeloid leukemia. Drug Resist Updat. 2022;61:100805.

2. Stomper J, Rotondo JC, Greve G, Lübbert M. Hypomethylating agents (HMA) for the treatment of acute myeloid leukemia and myelodysplastic syndromes: mechanisms of resistance and novel HMA-based therapies. Leukemia. 2021;35(7):1873-1889.

3. Liu H. Emerging agents and regimens for AML. J Hematol Oncol. 2021;14(1):49.

4. Pievani A, Donsante S, Tomasoni C, et al. Acute myeloid leukemia shapes the bone marrow stromal niche in vivo. Haematologica. 2021;106(3):865-870.

5. Barbier V, Erbani J, Fiveash C, et al. Endothelial E-selectin inhibition improves acute myeloid leukaemia therapy by disrupting vascular niche-mediated chemoresistance. Nat Commun. 2020;11(1):2042.

6. Chen T, Zhang G, Kong L, Xu S, Wang Y, Dong M. Leukemia-derived exosomes induced IL-8 production in bone marrow stromal cells to protect the leukemia cells against chemotherapy. Life Sci. 2019;221:187-195.

7. Hong CS, Jeong E, Boyiadzis M, Whiteside TL. Increased small extracellular vesicle secretion after chemotherapy via upregulation of cholesterol metabolism in acute myeloid leukaemia. J Extracell Vesicles. 2020;9(1):1800979.

8. Zhou H, Li Y, Liu B, et al. Downregulation of miR-224 and let-7i contribute to cell survival and chemoresistance in chronic myeloid leukemia cells by regulating ST3GAL IV expression. Gene. 2017;626:106-118.

9. Yu Y, Kou D, Liu B, et al. LncRNA MEG3 contributes to drug resistance in acute myeloid leukemia by positively regulating ALG9 through sponging miR-155. Int J Lab Hematol. 2020;42(4):464-472.

10. Feng H, Liang L, Deng W, Gao J, Li X, Guan F. Sialyl Lewis X decorated integrin α3 on small extracellular vesicles promotes metastasis of bladder cancer via enhancing vascular permeability. Angiogenesis. 2024;27(4):883-901.

11. Tan Z, Cao L, Wu Y, et al. Bisecting GlcNAc modification diminishes the pro-metastatic functions of small extracellular vesicles from breast cancer cells. J Extracell Vesicles. 2020;10(1):e12005.

12. Li H, Wang Y, Pang X, et al. Elevated TWIST1 expression in myelodysplastic syndromes/acute myeloid leukemia reduces efficacy of hypomethylating therapy with decitabine. Haematologica. 2020;105(10):e502.

13. Lei L, Wang Y, Liu R, et al. Transfer of miR-4755-5p through extracellular vesicles and particles induces decitabine resistance in recipient cells by targeting CDKN2B. Mol Carcinog. 2023;62(6):743-753.

14. Li M, Ye J, Xia Y, et al. METTL3 mediates chemoresistance by enhancing AML homing and engraftment via ITGA4. Leukemia. 2022;36(11):2586-2595.

15. Ninomiya M, Abe A, Katsumi A, et al. Homing, proliferation and survival sites of human leukemia cells in vivo in immunodeficient mice. Leukemia.

2007;21(1):136-142.

16. Fang JH, Zhang ZJ, Shang LR, et al. Hepatoma cell-secreted exosomal microRNA-103 increases vascular permeability and promotes metastasis by targeting junction proteins. Hepatology. 2018;68(4):1459-1475.

17. Lin Y, Zhang C, Xiang P, Shen J, Sun W, Yu H. Exosomes derived from HeLa cells break down vascular integrity by triggering endoplasmic reticulum stress in endothelial cells. J Extracell Vesicles. 2020;9(1):1722385.

18. Feng J, Wang Y, Li B, et al. Loss of bisecting GlcNAcylation on MCAM of bone marrow stoma determined pro-tumoral niche in MDS/AML. Leukemia. 2023;37(1):113-121.

19. Yi L, Hu Q, Zhou J, Liu Z, Li H. Alternative splicing of Ikaros regulates the FUT4/Le(X)-α5β1 integrin-FAK axis in acute lymphoblastic leukemia. Biochem Biophys Res Commun. 2019;510(1):128-134.

20. Spicer DB, Rhee J, Cheung WL, Lassar AB. Inhibition of myogenic bHLH and MEF2 transcription factors by the bHLH protein Twist. Science. 1996;272(5267):1476-1480.

21. Lee MS, Lowe GN, Strong DD, Wergedal JE, Glackin CA. TWIST, a basic helix-loop-helix transcription factor, can regulate the human osteogenic lineage. J Cell Biochem. 1999;75(4):566-577.

22. Braun T, Carvalho G, Fabre C, Grosjean J, Fenaux P, Kroemer G. Targeting NF-kappaB in hematologic malignancies. Cell Death Differ. 2006;13(5):748-758.

23. Cedervall J, Dimberg A, Olsson AK. Tumor-Induced Local and Systemic Impact

on Blood Vessel Function. Mediators Inflamm. 2015;2015:418290.

24. Li I, Nabet BY. Exosomes in the tumor microenvironment as mediators of cancer therapy resistance. Mol Cancer. 2019;18(1):32.

25. Bayat M, Sadri Nahand J. Exosomal miRNAs: the tumor's trojan horse in selective metastasis. Mol Cancer. 2024;23(1):167.

26. Shi J, Shen Y, Zhang J. Emerging roles of small extracellular vesicles in metabolic reprogramming and drug resistance in cancers. Cancer Drug Resist. 2024;7:38.

27. Wang ZF, Liao F, Wu H, Dai J. Glioma stem cells-derived exosomal miR-26a promotes angiogenesis of microvessel endothelial cells in glioma. J Exp Clin Cancer Res. 2019;38(1):201.

28. Lindoso RS, Collino F, Camussi G. Extracellular vesicles derived from renal cancer stem cells induce a pro-tumorigenic phenotype in mesenchymal stromal cells. Oncotarget. 2015;6(10):7959-7969.

29. Liu B, Ma H, Liu Q, et al. MiR-29b/Sp1/FUT4 axis modulates the malignancy of leukemia stem cells by regulating fucosylation via Wnt/β-catenin pathway in acute myeloid leukemia. J Exp Clin Cancer Res. 2019;38(1):200.

30. Giordano G, Febbraro A, Tomaselli E, et al. Cancer-related CD15/FUT4 overexpression decreases benefit to agents targeting EGFR or VEGF acting as a novel RAF-MEK-ERK kinase downstream regulator in metastatic colorectal cancer. J Exp Clin Cancer Res. 2015;34:108.

31. Cosset E, Hamdan G, Jeanpierre S, et al. Deregulation of TWIST-1 in the CD34+

compartment represents a novel prognostic factor in chronic myeloid leukemia. Blood. 2011;117(5):1673-1676.

32. Li H, Wang Y, Feng S, et al. Reciprocal regulation of TWIST1 and OGT determines the decitabine efficacy in MDS/AML. Cell Commun Signal. 2023;21(1):255.

33. Shen W, Xie J, Zhao S, et al. ICAM3 mediates inflammatory signaling to promote cancer cell stemness. Cancer Lett. 2018;422:29-43.

34. Gu P, Theiss A, Han J, Feagins LA. Increased Cell Adhesion Molecules, PECAM-1, ICAM-3, or VCAM-1, Predict Increased Risk for Flare in Patients With Quiescent Inflammatory Bowel Disease. J Clin Gastroenterol. 2017;51(6):522-527.

Figure legend

Fig. 1 The effect of decitabine (DAC) resistance on leukemic cell homing and endothelial permeability

(A) Xenotransplantation model. Mice were irradiated (3 Gy) and injected intravenously with KG1a or decitabine-resistant KG1a cells (KG1a-DAC). Human $CD45^+$ cells were quantified in blood, bone marrow, and spleen 16 h after injection (n = 6 mice per group). (B) Immunoblot analysis of tight junction proteins in human umbilical vein endothelial cells (HUVECs) incubated with plasma collected from healthy individuals (HD) and myelodysplastic syndromes/acute myeloid leukemia (MDS/AML) patients who were sensitive to decitabine (DAC) treatment (DAC-S) or refractory to DAC treatment (DAC-R). (C, D) HUVEC permeability to green fluorescent protein–positive (GFP^+) KG1a cells and rhodamine B–labeled dextran were examined after 48 h incubation with plasma from HD, DAC-S, and DAC-R MDS/AML patients. (E) Angiogenesis metrics, including junction count and total branching length, were quantified in HUVECs treated with the indicated plasma. Plasma samples: HD (n=15), DAC-S (n=15), DAC-R (n=15). Data are mean ± SEM; experiments were repeated three times with similar results. *P<0.05; **P<0.01; ***P<0.001.

Fig. 2 The effect of small extracellular vesicles (sEVs) released by decitabine (DAC)-resistant cells on leukemia cell homing and endothelial permeability

(A) Immunoblot analysis of tight junction–related proteins in HUVECs after exposure to sEVs from KG1a or KG1a-DAC. (B) HUVEC permeability after exposure to the indicated sEVs. (C) Angiogenesis metrics, including junction count and total

branching length, were quantified in HUVECs treated with the indicated sEVs. (D) Expression of tight junction–related proteins in HUVECs after exposure to sEVs from healthy individuals (HD) and myelodysplastic syndromes/acute myeloid leukemia (MDS/AML) patients who were sensitive to DAC treatment (DAC-S) or refractory to DAC treatment (DAC-R). (E) HUVEC permeability after exposure to the indicated sEVs. (F) Angiogenesis metrics, including junction count and total branching length, were quantified in HUVECs treated with the indicated sEVs. Plasma-derived sEV samples: HD (n=10), DAC-S (n=10), DAC-R (n=10). Data are mean ± SEM; experiments were repeated three times with similar results. *P<0.05; **P<0.01; ***P<0.001.

Fig. 3 Analysis of fucosylation and fucosyltransferases (FUTs) expression in myelodysplastic syndromes/acute myeloid leukemia (MDS/AML) patients who were sensitive to decitabine (DAC) treatment (DAC-S) or refractory to DAC treatment (DAC-R)

(A) Lectin blotting analysis of core fucose (LCA) and terminal fucose (AAL) in plasma-derived small extracellular vesicles (sEVs) from HD, DAC-S and DAC-R patients; band intensities were normalized to TSG101. (B) Relative levels of AAL on sEVs determined by ELISA. (C, D) Lectin blotting analysis of LCA and AAL in KG1a, KG1a-DAC cells and their derived sEVs; band intensities were normalized to GAPDH (cell lysates) or TSG101 (sEVs), as indicated. (E) Relative expression of FUTs in KG1a and KG1a-DAC measured by quantitative reverse transcription PCR (qRT-PCR). Plasma-derived sEV samples: HD (n=15), DAC-S (n=15), DAC-R (n=15).

Data are mean ± SEM; experiments were repeated three times with similar results. ns, not significant; *P<0.05; **P<0.01; ***P<0.001.

Fig. 4 Impact of Lewis^{x} (Le^{x}) expression on leukemic cell homing and vascular permeability

(A) Schematic illustration of Le^{X} and FUT4-mediated Le^{X} modification. (B) Le^{X} levels in KG1a and KG1a-DAC cells and their derived small extracellular vesicles (sEVs). (C) Fucosyltransferase 4 (FUT4) expression and Le^{X} levels in KG1a cells overexpressing FUT4 (designated as KG1a-FUT4) and their sEVs. (D) Tight junction–related proteins in HUVECs treated with sEVs from KG1a and KG1a-FUT4. (E) HUVEC permeability and leukemic cell transendothelial migration after treatment with sEVs from KG1a or KG1a-FUT4. (F) Angiogenesis metrics, including junction count and total branching length, were quantified in HUVECs treated with sEVs from KG1a or KG1a-FUT4. (G) Schematic of the xenotransplantation mouse model and quantification of human CD45^{+} cells in blood, bone marrow, and spleen. Data are mean ± SEM; experiments were repeated three times with similar results. *P<0.05; **P<0.01; ***P<0.001.

Fig. 5 TWIST1 activated fucosyltransferase 4 (FUT4) transcription

(A) Expression of FUT4, TWIST1 and the levels of Le^{X} in KG1a and KG1a cells overexpressing TWIST1 (KG1a-TWIST1). (B) Tight junction–related proteins and (C) HUVEC permeability and leukemic cell transendothelial migration after treatment with conditioned medium (CM) from KG1a or KG1a-TWIST1 cells. (D) Angiogenesis metrics, including junction count and total branching length, were quantified in HUVECs treated with CM from KG1a or KG1a-TWIST1 cells. (E) ChIP analysis of

TWIST1 binding to E-box motifs within the *FUT4* promoter (0–2000 bp). GAPDH was used as negative control. (F) Dual luciferase assay of TWIST1 binding to wild-type and mutant E-box motifs. Data are mean ± SEM; experiments were repeated three times with similar results. ns, not significant; *P<0.05; **P<0.01; ***P<0.001.

Fig. 6 Effects of Lewis^x (Le^x)-modified intercellular adhesion molecule 3 (ICAM3) on vascular permeability and leukemic cell homing

(A) Venn diagram showing differentially expressed proteins among parental KG1a cells, decitabine-resistant KG1a (KG1a-DAC) cells, fucosyltransferase 4–overexpressing KG1a (KG1a-FUT4) cells, and FUT4-silenced KG1a-DAC (KG1a-DAC-shFUT4) cells. (B) LC-MS analysis of ICAM3 in these cells. (C) Le^x modification on ICAM3 evaluated by IP/western blotting. (D) Expression of tight junction–related proteins and NF-κB signaling components (p65, p-p65, IκBα, p-IκBα) in KG1a, KG1a-DAC and KG1a-DAC treated with anti-human ICAM3 antibody (a-ICAM3). (E) Cell permeability and (F) angiogenesis metrics of HUVEC after coculture with KG1a, KG1a-DAC or KG1a-DAC in the presence of a-ICAM3. Data are mean ± SEM; experiments were repeated three times with similar results. *P<0.05; **P<0.01; ***P<0.001.

Fig. 7 Lewis^x-modified intercellular adhesion molecule 3 (ICAM3) on small extracellular vesicles (sEVs) mediated endothelial dysfunction promotes leukemic cell homing in decitabine (DAC)-resistant myelodysplastic syndromes/acute myeloid leukemia (MDS/AML) (conceptual model)

Figure1

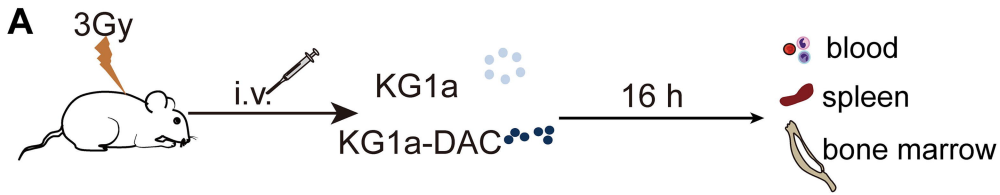
A
3Gy
i.v.
KG1a
KG1a-DAC
16 h
blood
spleen
bone marrow

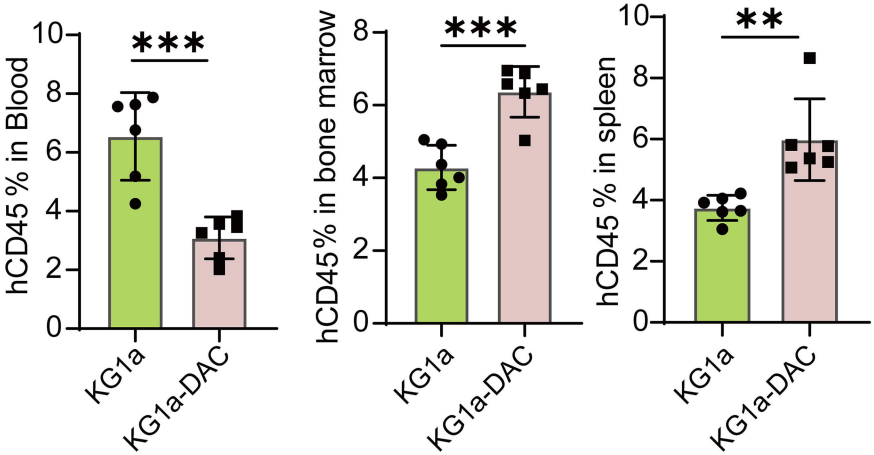
hCD45 % in Blood
***
KG1a
KG1a-DAC
hCD45% in bone marrow
***
KG1a
KG1a-DAC
hCD45 % in spleen
**
KG1a
KG1a-DAC

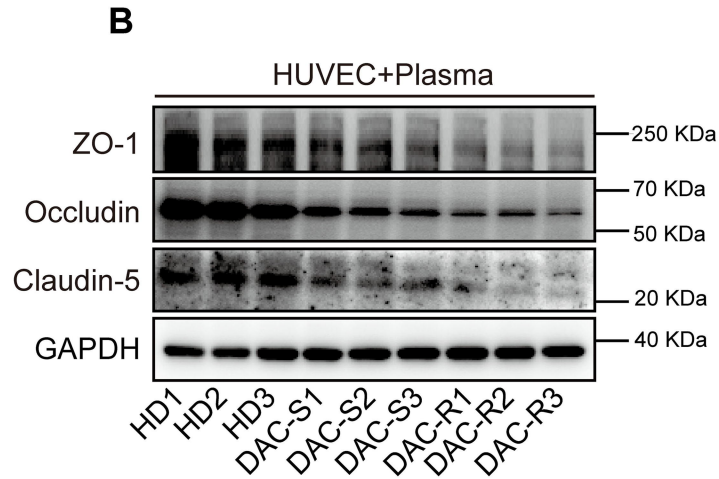
B
HUVEC+Plasma
ZO-1
Occludin
Claudin-5
GAPDH
250 KDa
70 KDa
50 KDa
20 KDa
40 KDa
HD1
HD2
HD3
DAC-S1
DAC-S2
DAC-S3
DAC-R1
DAC-R2
DAC-R3

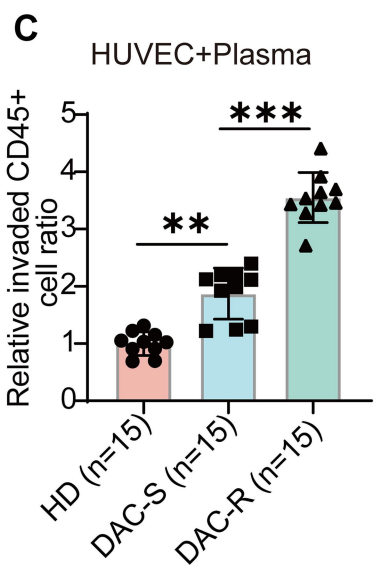
C
HUVEC+Plasma
Relative invaded CD45+ cell ratio
**
***
HD (n=15)
DAC-S (n=15)
DAC-R (n=15)

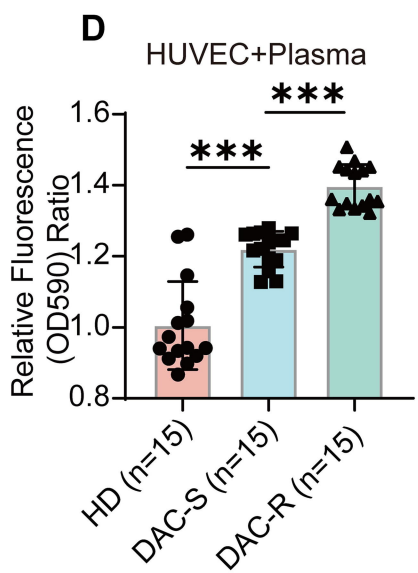
D
HUVEC+Plasma
Relative Fluorescence (OD590) Ratio
***
***
HD (n=15)
DAC-S (n=15)
DAC-R (n=15)

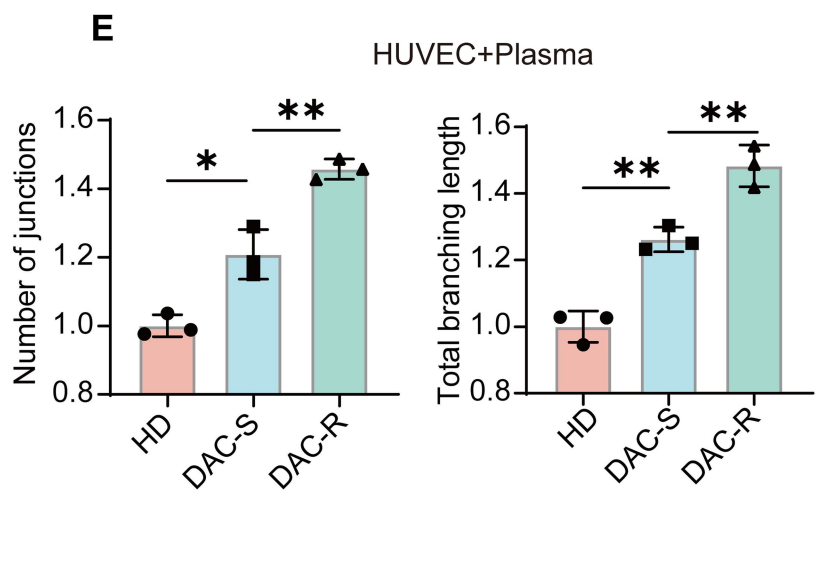
E
HUVEC+Plasma
Number of junctions
*
**
HD
DAC-S
DAC-R
Total branching length
**
**
HD
DAC-S
DAC-R

Figure2

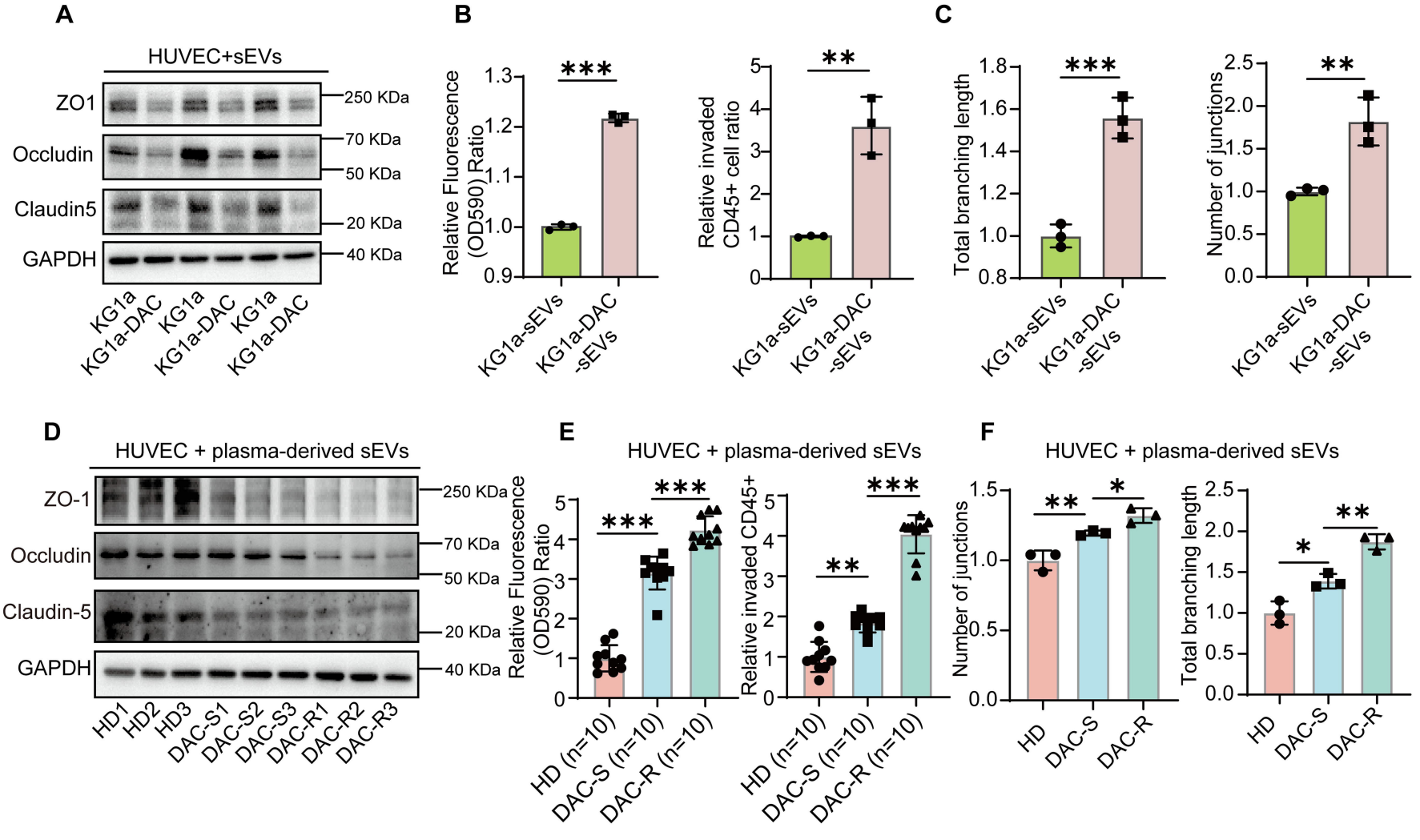
A
HUVEC+sEVs
ZO1
Occludin
Claudin5
GAPDH
250 KDa
70 KDa
50 KDa
20 KDa
40 KDa
KG1a
KG1a-DAC
B
Relative Fluorescence (OD590) Ratio
Relative invaded CD45+ cell ratio
KG1a-sEVs
KG1a-DAC -sEVs
C
Total branching length
Number of junctions
D
HUVEC + plasma-derived sEVs
ZO-1
Occludin
Claudin-5
GAPDH
HD1
HD2
HD3
DAC-S1
DAC-S2
DAC-S3
DAC-R1
DAC-R2
DAC-R3
E
HUVEC + plasma-derived sEVs
HD (n=10)
DAC-S (n=10)
DAC-R (n=10)
F
HUVEC + plasma-derived sEVs
HD
DAC-S
DAC-R

Figure3

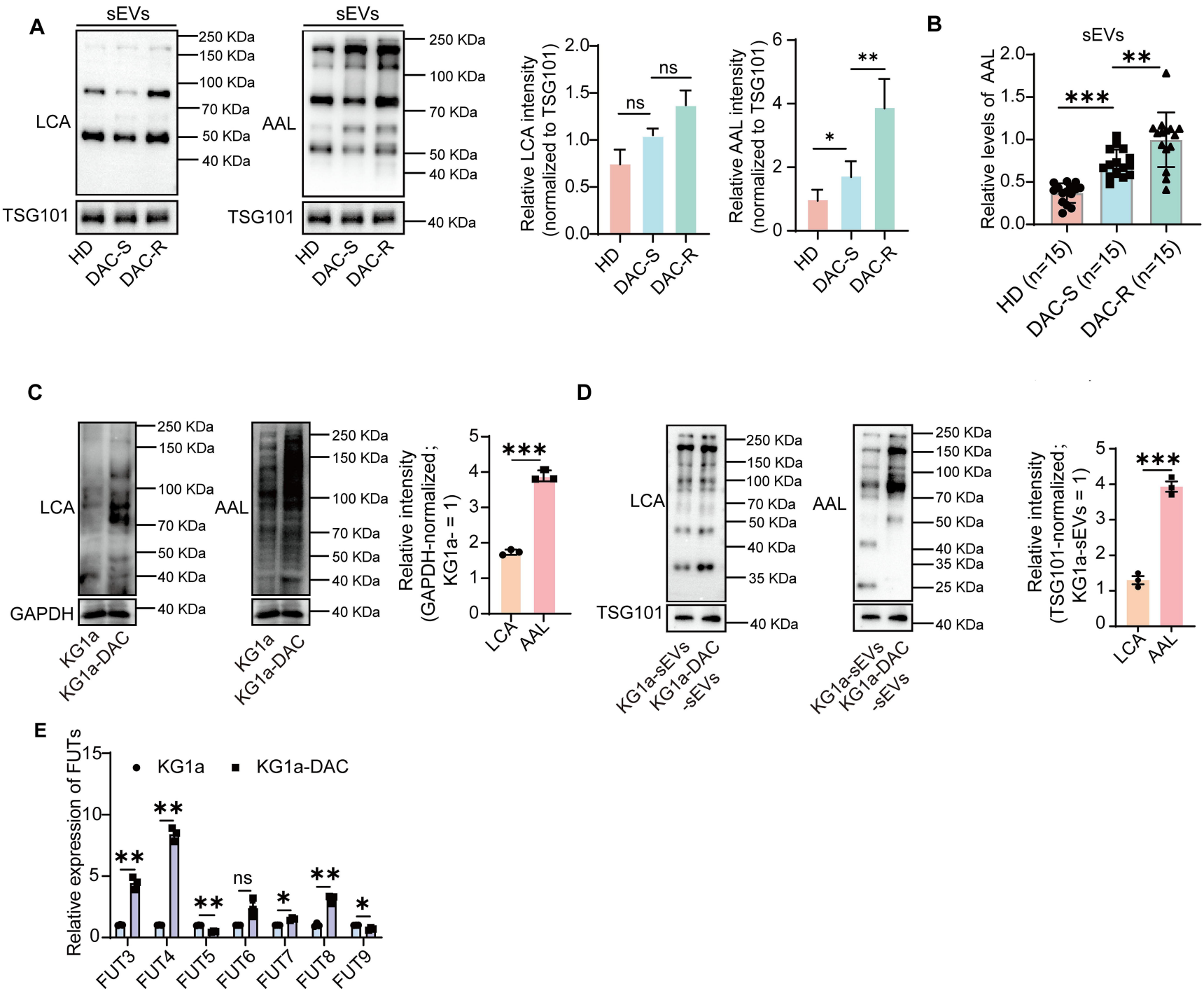
A
sEVs
LCA
TSG101
250 KDa
150 KDa
100 KDa
70 KDa
50 KDa
40 KDa
HD
DAC-S
DAC-R
AAL
Relative LCA intensity (normalized to TSG101)
Relative AAL intensity (normalized to TSG101)
ns
*
**
B
Relative levels of AAL
***
HD (n=15)
DAC-S (n=15)
DAC-R (n=15)
C
GAPDH
KG1a
KG1a-DAC
Relative intensity (GAPDH-normalized; KG1a- = 1)
LCA
AAL
D
35 KDa
25 KDa
KG1a-sEVs
KG1a-DAC -sEVs
Relative intensity (TSG101-normalized; KG1a-sEVs = 1)
E
KG1a
KG1a-DAC
Relative expression of FUTs
FUT3
FUT4
FUT5
FUT6
FUT7
FUT8
FUT9

Figure4

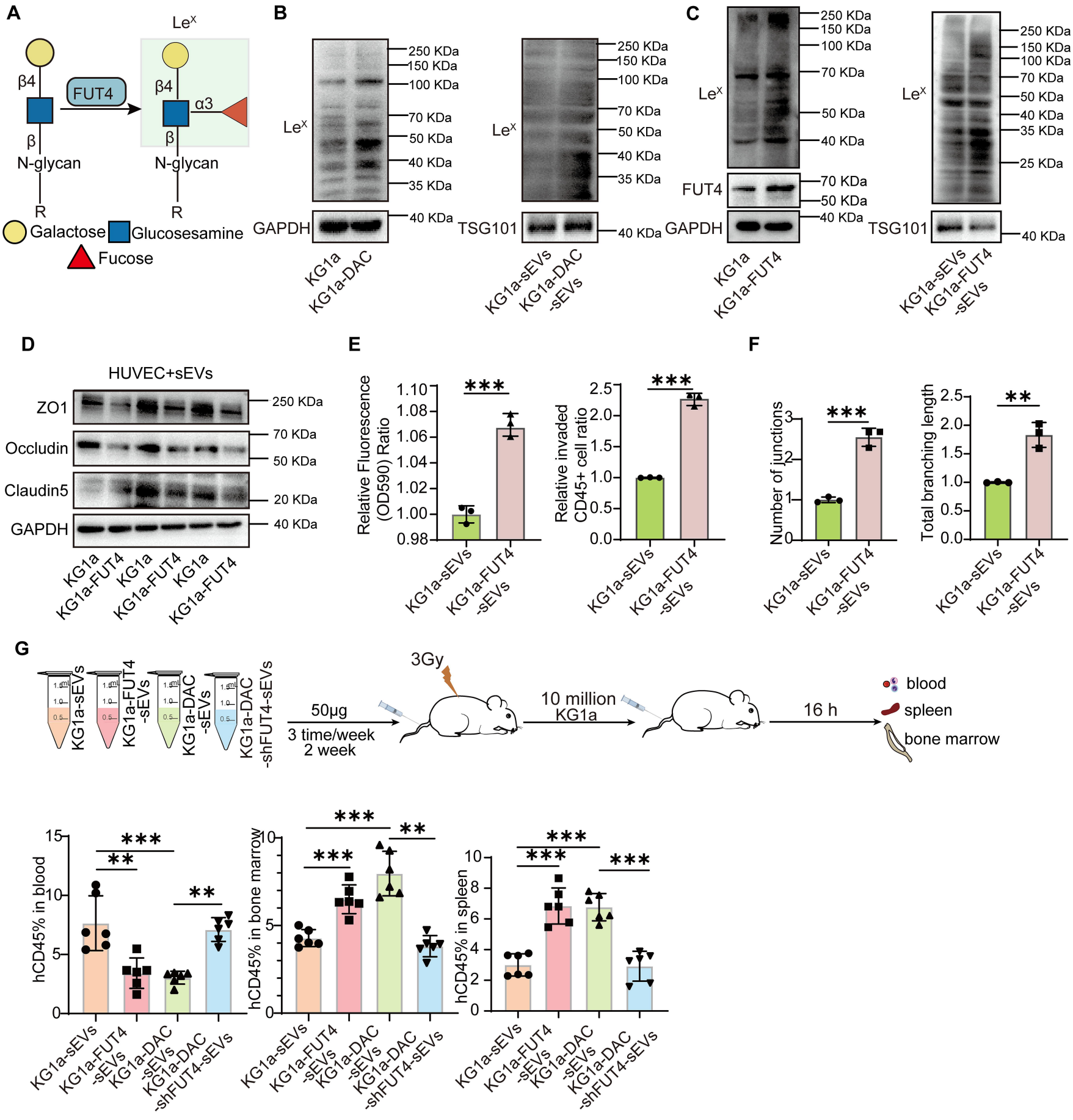
A
Le^X
β4
FUT4
β4
α3
β
β
N-glycan
N-glycan
R
R
Galactose
Glucosesamine
Fucose
B
Le^X
250 KDa
150 KDa
100 KDa
70 KDa
50 KDa
40 KDa
35 KDa
GAPDH
40 KDa
KG1a
KG1a-DAC
Le^X
TSG101
KG1a-sEVs
KG1a-DAC -sEVs
C
Le^X
FUT4
GAPDH
KG1a
KG1a-FUT4
TSG101
KG1a-sEVs
KG1a-FUT4 -sEVs
D
HUVEC+sEVs
ZO1
Occludin
Claudin5
GAPDH
20 KDa
KG1a
KG1a-FUT4
E
Relative Fluorescence (OD590) Ratio
Relative invaded CD45+ cell ratio
***
KG1a-sEVs
KG1a-FUT4 -sEVs
F
Number of junctions
Total branching length
**
G
KG1a-sEVs
KG1a-FUT4 -sEVs
KG1a-DAC -sEVs
KG1a-DAC -shFUT4-sEVs
50μg
3 time/week
2 week
3Gy
10 million KG1a
16 h
blood
spleen
bone marrow
hCD45% in blood
hCD45% in bone marrow
hCD45% in spleen

Figure5

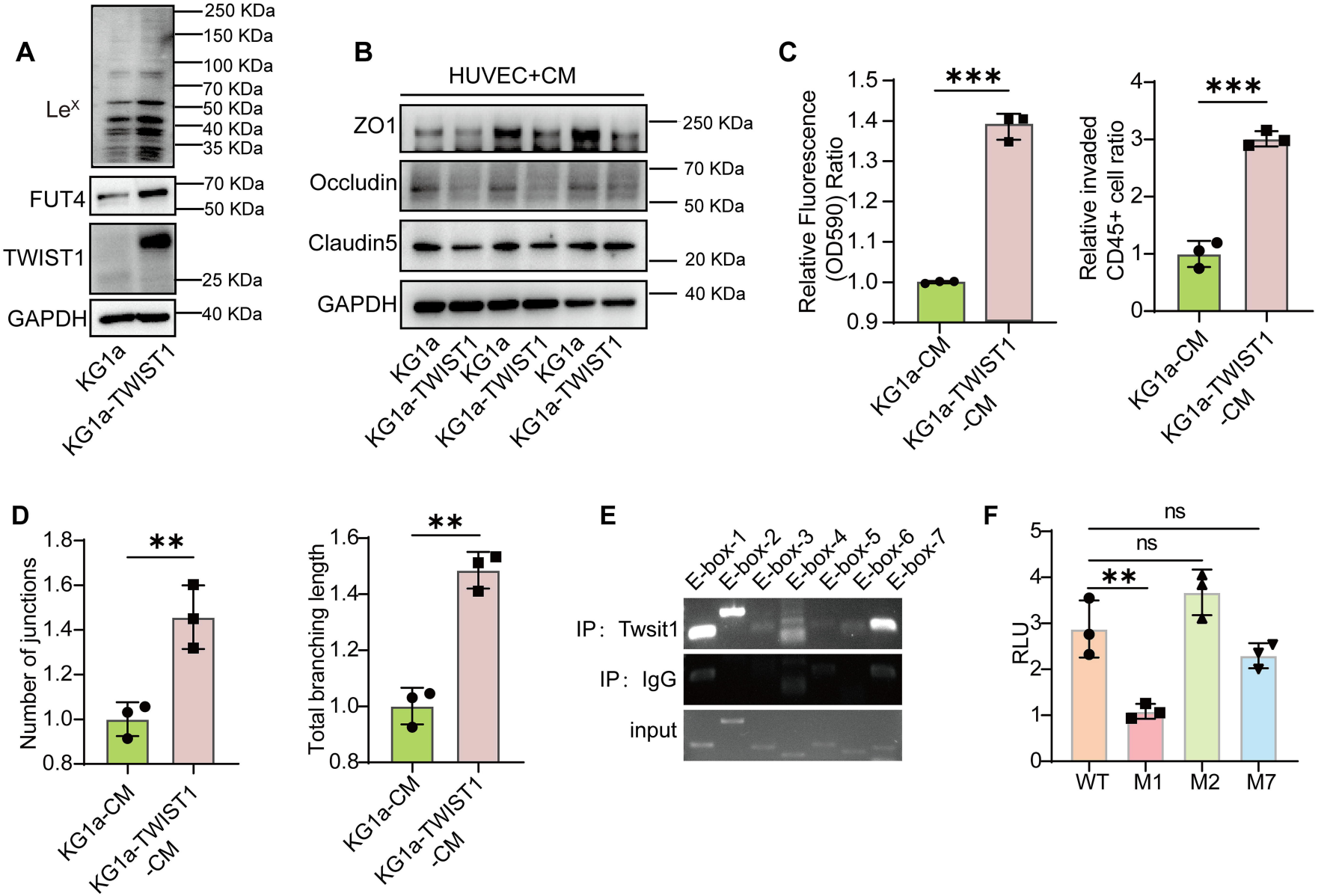
A
250 KDa
150 KDa
100 KDa
70 KDa
50 KDa
40 KDa
35 KDa
Le^X
70 KDa
50 KDa
FUT4
TWIST1
25 KDa
GAPDH
40 KDa
KG1a
KG1a-TWIST1
B
HUVEC+CM
ZO1
250 KDa
Occludin
70 KDa
50 KDa
Claudin5
20 KDa
GAPDH
40 KDa
KG1a
KG1a-TWIST1
KG1a
KG1a-TWIST1
KG1a
KG1a-TWIST1
C
***
Relative Fluorescence (OD590) Ratio
1.5
1.4
1.3
1.2
1.1
1.0
0.9
KG1a-CM
KG1a-TWIST1 -CM
***
Relative invaded CD45+ cell ratio
4
3
2
1
0
KG1a-CM
KG1a-TWIST1 -CM
D
**
Number of junctions
1.8
1.6
1.4
1.2
1.0
0.8
KG1a-CM
KG1a-TWIST1 -CM
**
Total branching length
1.6
1.4
1.2
1.0
0.8
KG1a-CM
KG1a-TWIST1 -CM
E
E-box-1
E-box-2
E-box-3
E-box-4
E-box-5
E-box-6
E-box-7
IP: Twsit1
IP: IgG
input
F
ns
ns
**
RLU
5
4
3
2
1
0
WT
M1
M2
M7

Figure6

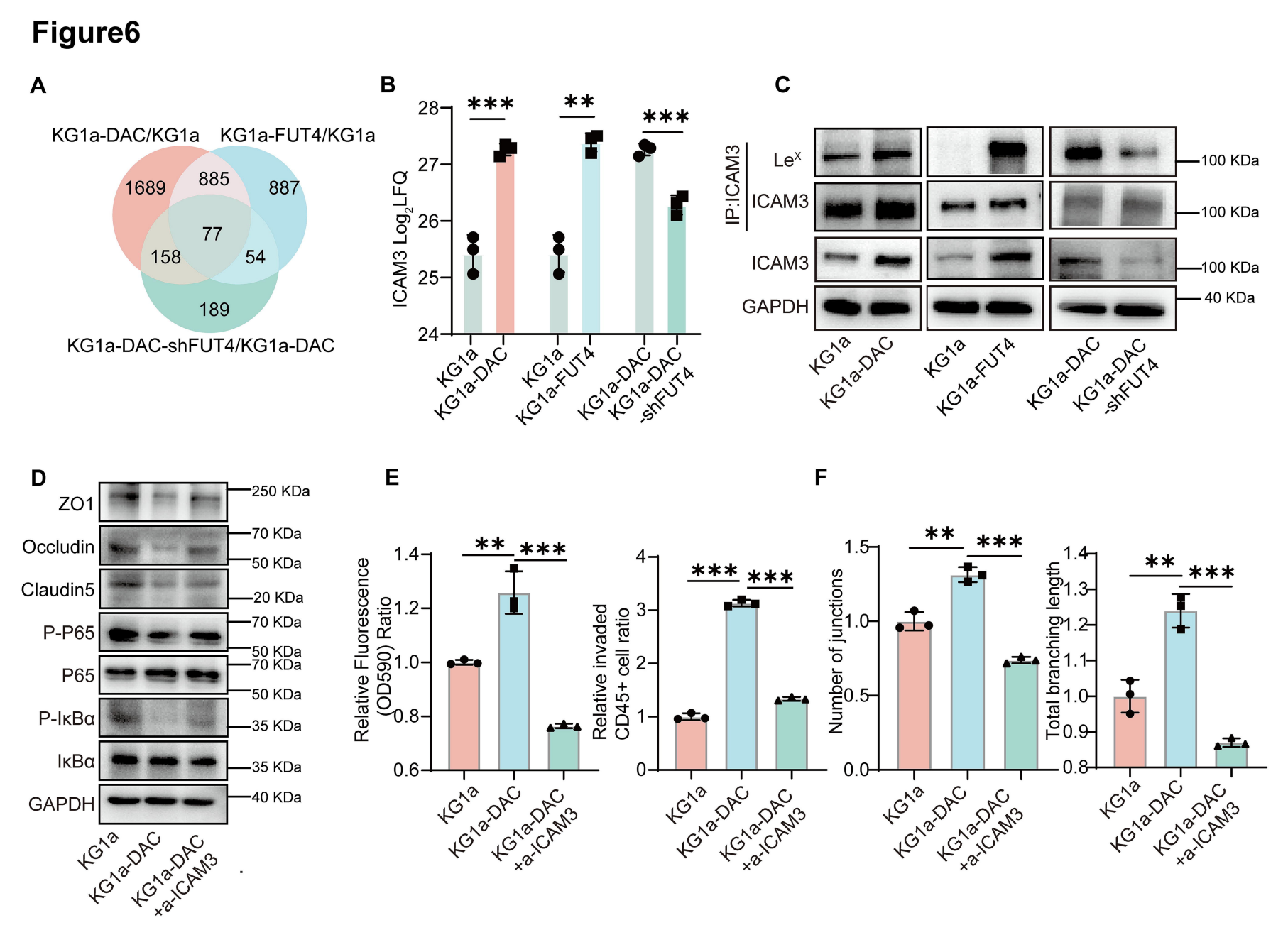
A
KG1a-DAC/KG1a
KG1a-FUT4/KG1a
1689
885
887
77
158
54
189
KG1a-DAC-shFUT4/KG1a-DAC
B
ICAM3 Log2LFQ
28
27
26
25
24
***
**
***
KG1a
KG1a-DAC
KG1a
KG1a-FUT4
KG1a-DAC
KG1a-DAC -shFUT4
C
IP:ICAM3
Le^X
ICAM3
ICAM3
GAPDH
100 KDa
100 KDa
100 KDa
40 KDa
KG1a
KG1a-DAC
KG1a
KG1a-FUT4
KG1a-DAC
KG1a-DAC -shFUT4
D
ZO1
Occludin
Claudin5
P-P65
P65
P-IκBα
IκBα
GAPDH
250 KDa
70 KDa
50 KDa
20 KDa
70 KDa
50 KDa
70 KDa
50 KDa
35 KDa
35 KDa
40 KDa
KG1a
KG1a-DAC
KG1a-DAC +a-ICAM3
E
Relative Fluorescence (OD590) Ratio
1.4
1.2
1.0
0.8
0.6
**
***
Relative invaded CD45+ cell ratio
4
3
2
1
0
***
***
KG1a
KG1a-DAC
KG1a-DAC +a-ICAM3
F
Number of junctions
1.5
1.0
0.5
0.0
**
***
Total branching length
1.4
1.3
1.2
1.1
1.0
0.9
0.8
**
***
KG1a
KG1a-DAC
KG1a-DAC +a-ICAM3

Figure7

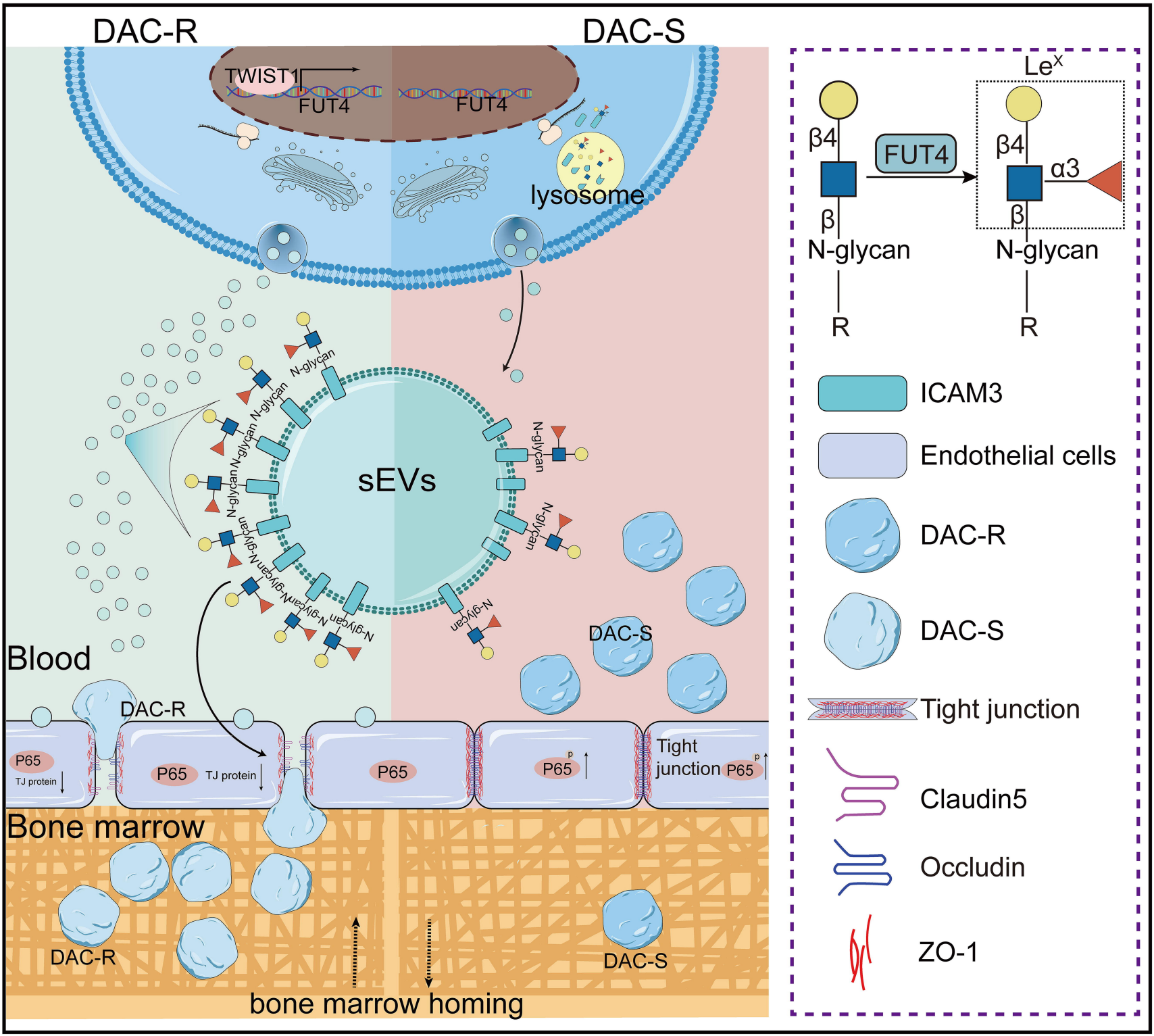
DAC-R
DAC-S
TWIST1
FUT4
FUT4
lysosome
N-glycan
sEVs
Blood
DAC-R
DAC-S
P65
TJ protein
P65
TJ protein
P65
P65
Tight junction
P65
Bone marrow
DAC-R
DAC-S
bone marrow homing
Le^x
β4
β
N-glycan
R
FUT4
β4
α3
β
N-glycan
R
ICAM3
Endothelial cells
DAC-R
DAC-S
Tight junction
Claudin5
Occludin
ZO-1

Aberrant fucosylation of extracellular vesicles remodels the vascular microenvironment and promotes chemoresistance in myelodysplastic syndromes and acute myeloid leukemia

Jingjing Feng[1,2#], Kexin Wang[1#], Junjie Gou[1,3#], Yi Wang[4], Bowen Hu[1], Wei Wei[1], Junqi Ge[1], Yanli Feng[4], Shuang Feng[1], Eric Solary[2], Feng Guan[1], Xiang Li[1,5*]

1. Key Laboratory of Resource Biology and Biotechnology of Western China, Ministry of Education; Provincial Key Laboratory of Biotechnology, College of Life Sciences, Northwest University, Xi'an, China.
2. INSERM U1287, Université Paris-Saclay, Gustave Roussy Cancer Center, Villejuif, France.
3. Xi'an No. 1 Hospital, First Affiliated Hospital of Northwest University, School of Medicine, Xi'an, China.
4. Department of Hematology, Provincial People's Hospital, Xi'an, China.
5. Institute of Hematology, School of Medicine, Northwest University, Xi'an, China.

The authors have declared that no conflict of interest exists.

# Authors contributed equally.

*Correspondence to Xiang Li (e-mail: xiangli@nwu.edu.cn), Tel: +86-29-88303534, College of Life Science, Northwest University, 229 Taibai North Road, Xi'an, Shaanxi 710069, China

Supplemental methods

Cell lines and cell culture

Human leukemia-derived cell line KG1a and DAC-resistant KG1a (KG1a-DAC)[1] were cultured in RPMI 1640 medium, human umbilical vein endothelial cell line HUVEC and embryonic kidney cell line HEK-293T were cultured in DMEM (Biological Industries; Kibbutz Beit Haemek, Israel). All medium was supplemented with 10% fetal bovine serum (FBS) (Biological Industries). All cells were maintained at 37°C in a 5% CO_2 atmosphere and routinely tested for Mycoplasma with the GMyc-PCR Mycoplasma Test Kit (#40601ES20, Yeasen, Shanghai, China).

Preparation of conditioned medium (CM) and sEVs

Cells were incubated in FBS-free medium for 48 h. The supernatant was collected and centrifuged at 500 × g for 10 min, and then filtered with 0.22 μm filter as CM.

To prepare sEVs, CM was sequentially centrifuged at 2000 × g for 20 min, 10,000×*g* for 30 min at 4 °C, and ultracentrifuged twice at 100,000 × g (Optima XE-100; Beckman Coulter Life Sciences; Indianapolis, IN, USA) for 70 min.[2] Pellets were resuspended in PBS and stored at -80 °C.

Characterization of sEVs

Isolated sEVs were placed on 400-mesh carbon-coated grids (Electron Microscopy Sciences; Fort Washington, PA, USA) and stained with 2% uranyl acetate. Images were captured using a transmission electron microscopy (TEM) (model H-7650; Hitachi; Tokyo). Nanoparticle tracking analysis (NTA) was performed using the Zetaview-PMX120-Z instrument (Particle Metrix, Meerbusch, Germany).

Permeability assay

HUVECs (6×10^4) were plated on 0.4 μm transwell filters in a 12-well plate (Jet Biofil), and treated with CM or sEVs (50 μg/mL) for 48 h. Rhodamine B (RB)-dextran (70 kDa; Sigma-Aldrich, St. Louis, MO, USA) was added to the upper well to a final concentration of 10 μg/mL. Following an incubation period of 30 minutes, the fluorescence intensity in the lower chamber was quantified using a microplate reader, with an excitation wavelength at 544 nm and an emission wavelength at 590 nm.

Transendothelial migration analysis

HUVECs (3×10^4) were plated on 8 μm transwell filters in a 12-well plate (Jet Biofil) to form a monolayer, and treated with CM or sEVs (50 μg/mL) for 48 h. Subsequently, 1×10^4 stable GFP-expressing KG1a cells were added into upper chamber and cultured for 24 h. Afterward, the cells migrated to the lower chamber were harvested, and the GFP fluorescence intensity of these cells was assessed using flow cytometry.

Tube formation assay

HUVECs were incubated with serum-free medium for 12 h, and then seeded at 2×10^4 cells per well in 96-well plates precoated with Matrigel matrix (Corning, NY, USA). These cells were treated with CM or sEVs (50 μg/mL) for 4–6 h. Tube formation was observed and documented photographically under a microscope.

SDS-PAGE and Western blotting

Cells were collected and lysed with RIPA buffer (50 mM Tris, pH 7.2, 1% Triton X-100, 0.5% sodium deoxycholate, 0.1% SDS, 150 mM NaCl, 10 mM $MgCl_2$ and 5% glycerol) containing 1% PMSF. Protein concentration was determined using BCA

Protein Assay Kit (#P0011, Beyotime, Nanjing, China). Proteins (25 μg) from each lysate were separated by electrophoresis in a 10% polyacrylamide resolving gel and transferred onto a polyvinylidene difluoride (PVDF) membranes. After blocking with 3% BSA (#ST023, Beyotime) in Tris-buffered saline containing 0.1% Tween-20 (TBST) at RT for 1 h, membranes were incubated at 4°C overnight in TBS-T containing following antibodies against Alix (#92880S, Cell Signaling Technology, MA, USA), Calnexin (#2679S), IκBα (#9242), p65 (#8242), p- IκBα (#2859), p- p65 (#3031), FUT4 (#19497-1-AP, proteintech, Wuhan, China), CD15 (#sc-19595), Occludin (#sc-133256), Claudin-5 (#sc-374221), ZO1 (#sc-33725, Santa Cruz Biotechnology, USA), TSG101 (#T55985, Abmart, Shanghai, China), followed by the addition of secondary antibody conjugated with HRP (#A0208, #A0216, Beyotime). Bands were visualized by enhanced chemiluminescence (ECL; Vazyme Biotech, Nanjing, China).

Detection of Le^X on sEVs by lectin-based ELISA

To determine the levels of Le^X on sEVs, 96-well ELISA plates were pre-coated with 100 μL/well of anti-CD63 antibody (sc-365604, Santa Cruz Biotechnology) and incubated for 12 h at 4 °C. The plates were washed three times with PBST (0.05% Tween-20 in PBS) and blocked with 1% BSA for 1 h at 37 °C. sEVs samples were added and incubated for 2 h at 37 °C. After washing with PBST, the wells were incubated with biotinylated Aleuria aurantia lectin for 2 h at 37 °C, followed by incubation with HRP-conjugated streptavidin for 30 min at 37 °C. The plates were developed using 3,3′,5,5′-tetramethylbenzidine (TMB) substrate (Promega, Madison, USA) and the reaction was stopped with 2 M H_2SO_4. Absorbance was measured at

450 nm using a microplate reader.

Proteomic analysis

Proteins (100 µg) were denatured with 8 M urea, reduced by 5 mM dithiothreitol (DTT) for 1 h at RT, alkylated with 20 mM iodoacetamide (IAM) for 30 min in the dark at RT, diluted with deionized water to lower urea concentration below 2 M, digested with lysyl endopeptidase (Wako Puro Chemical; Osaka, Japan) for 4 h at 37 °C, and digested with trypsin (Promega) overnight at 37 °C. The mixture was acidified with 10% trifluoroacetic acid (TFA) to pH< 3 and purified using C18 cartridges (Waters Corp.; Taunton, MA, USA). Two-dimensional liquid chromatography/ mass spectrometry (LC-MS) was performed on LTQ8 Orbitrap MS (Thermo Fisher; San Jose, CA, USA) and data were analyzed using Proteome Discoverer software (Thermo Fisher), with quantification by MaxQuant software program v2.6.7.0 (maxquant.org).[3]

N-glycan analysis

Glycomic analysis was performed as previously described.[4] A volume of 10 µL serum or 1 mg of sEVs was added onto a size-exclusion spin ultrafiltration unit (Millipore; Billerica, MA, USA). Proteins were denatured with 8 M urea/ 50 mM NH4HCO3, reduced with dithiothreitol (DTT), alkylated with iodoacetamide (IAM), and digested with PNGase F overnight at 37 °C. Released N-glycans were collected by centrifugation, lyophilized, and desalted using HyperSep Hypercarb solid phase extraction (SPE) cartridge (ThermoFisher Scientific; Waltham, Massachusetts, US).

Lyophilized N-glycans were dissolved and spotted onto an MTP AnchorChip sample target with 20 mg/mL 2,5-dihydroxybenzoic acid (DHB) as the matrix.

Measurements were taken in positive-ion mode. Each full-mass scan was performed with following conditions: acceleration voltage, 24.59 kV; reflector voltage, 26.6 kV; pulsed ion extraction, 100 ns; mass range, 1000–3500 m/z. For the data analysis, the peaks were smoothed and baseline subtraction performed three times. Relative intensity was analyzed and generated using FlexAnalysis software (Bruker Daltonics; Bremen, Germany) based on MALDI-TOF/TOF–MS intensity. m/z data were annotated using GlycoWorkbench software,[5] and cross-referenced with previous studies. [6-8]

Chromatin immunoprecipitation assay (ChIP)

The ChIP assay was performed as described previously.[9] Briefly, KG1a-TWIST1 cells[10] were cross-linked with 1% formaldehyde. Subsequently, DNA was fragmented to an average length of 200 to 500 bp using a sonicator (#Ymnl-1000Y, Nanjing, China). Immunoprecipitation was performed using antibody against TWIST1 (#ab50887, Abcam). Protein A/G agarose was added and rotated for 4 h. The samples were subsequently treated with proteinase K (#ST532, Beyotime) and RNase A (#ST578, Beyotime). Target DNA was extracted using phenol/chloroform and analyzed by PCR with the primers in Tab. S2.

Dual luciferase reporter assay

The wild type and mutant regions of FUT4 promoter were amplified by PCR and cloned into pGL3 vector (#E1751, Promega; Madison, WI, USA). Then the pGL3 vector containing the wild-type or mutant FUT4 promoter regions was co-transfected into HEK-293T cells along with the Renilla luciferase expression plasmid (pRL-TK, #D2760, Beyotime) and the TWIST1 overexpression plasmid. After 48 h, luciferase activity was

measured with a Dual Luciferase Reporter Assay System (#RG028, Beyotime). The primers for PCR have been shown in Tab.S3.

OptiPrep density gradient purification

sEVs were purified by OptiPrep density gradient as described previously.[11] In brief, 40%, 20%, 10%, and 5% (w/v) iodixanol solutions were prepared by diluting OptiPrep (60% (w/v) aqueous iodixanol, Axis-Shield PoC; AS; Oslo, Norway) with 0.25 M sucrose/ 10 mM Tris, pH 7.5 in 14 × 89 mm Ultra-Clear tubes. sEVs purified by ultracentrifugation were placed on top of the gradient, continuous gradient was established through ultracentrifugation at 100,000 × g for 18 h using a Beckman Coulter Optima XE-100 and Ti45 rotor, and twelve fractions were collected. Each fraction was diluted in PBS, pelleted through another round of ultracentrifugation at 100,000 x g for 3 h, and washed with and resuspended in PBS.

Supplementary figures with legends.

Fig. S1. (A) Permeability of HUVEC monolayers to rhodamine B–labeled dextran (RB-dextran) after coculture with KG1a or KG1a-DAC for 48 h. (B) Immunoblot analysis of tight junction proteins in HUVECs cocultured with KG1a or KG1a-DAC. (C) Representative images of tube formation. (D) Immunoblot analysis of tight junction–related proteins in HUVECs treated with conditioned medium (CM) from KG1a or KG1a-DAC. (E) RB-dextran permeability and (F) transendothelial migration after CM treatment. (G) Quantification of junction count and total branching length in HUVECs treated with CM. Data are mean ± SEM; experiments were repeated three times with similar results. **P<0.01; ***P<0.001.

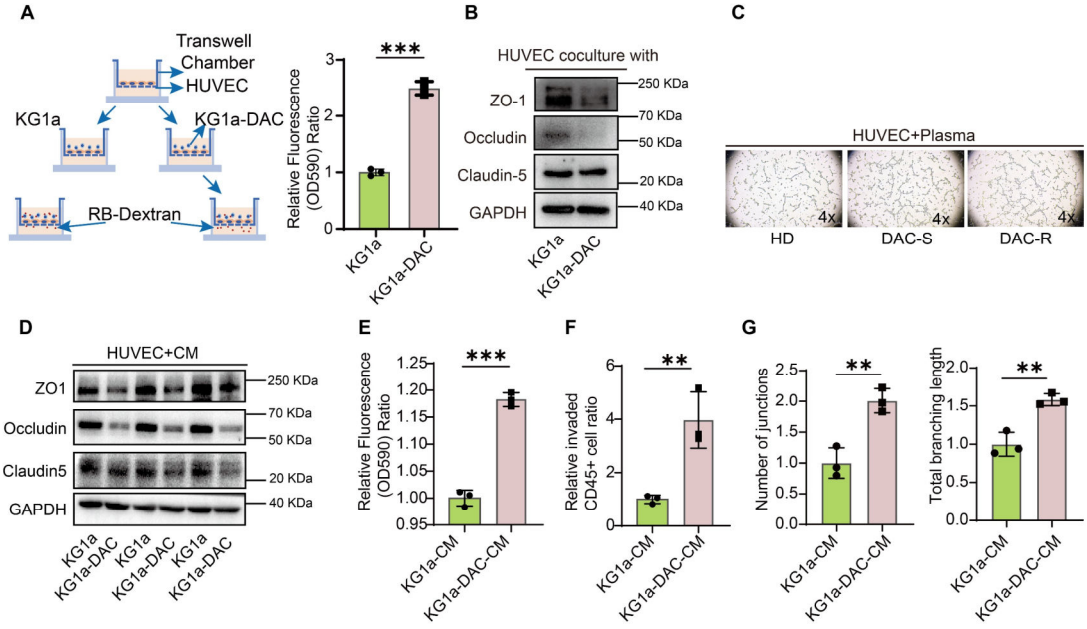

Fig. S2. (A-F) Characteristic of small extracellular vesicles (sEVs) using TEM (A&B), NTA (C&D), and western blotting (E&F). (G)Tube formation assay.

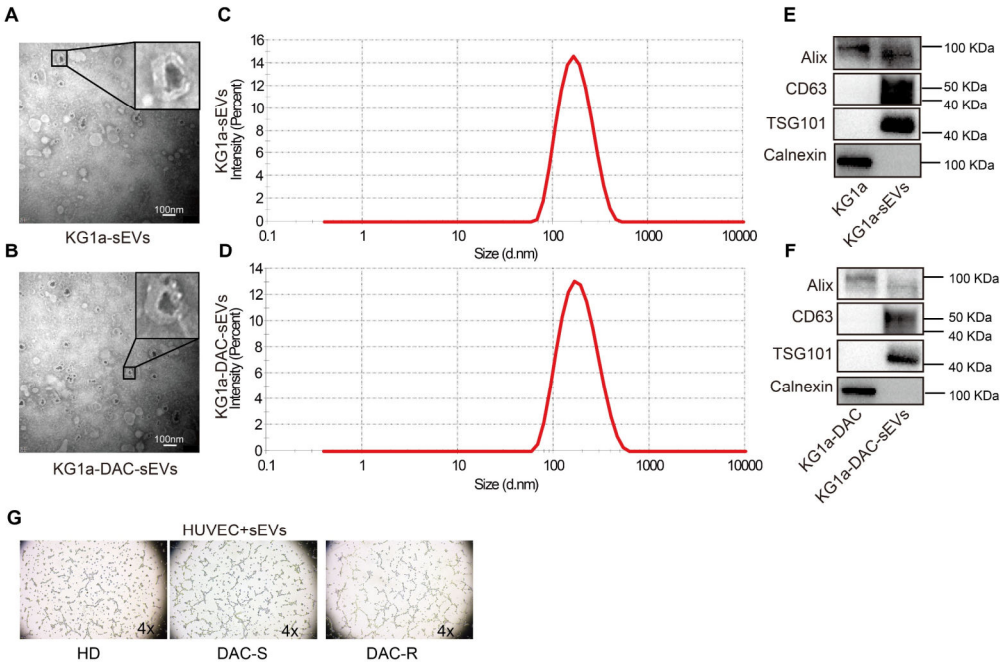

Fig. S3. (A-C) MALDI-TOF/TOF–MS spectra of N-glycans in myelodysplastic syndromes/acute myeloid leukemia (MDS/AML) patients who are sensitive to DAC treatment (DAC-S) or are refractory to DAC treatment (DAC-R) serum samples. Peaks

of MALDI-TOF/TOF–MS spectra (signal-to-noise ratio>5) were selected for relative intensity analysis. Glycan compositions are annotated using the H/N/F/S nomenclature (H, hexose; N, N-acetylglucosamine; F, fucose; S, sialic acid).

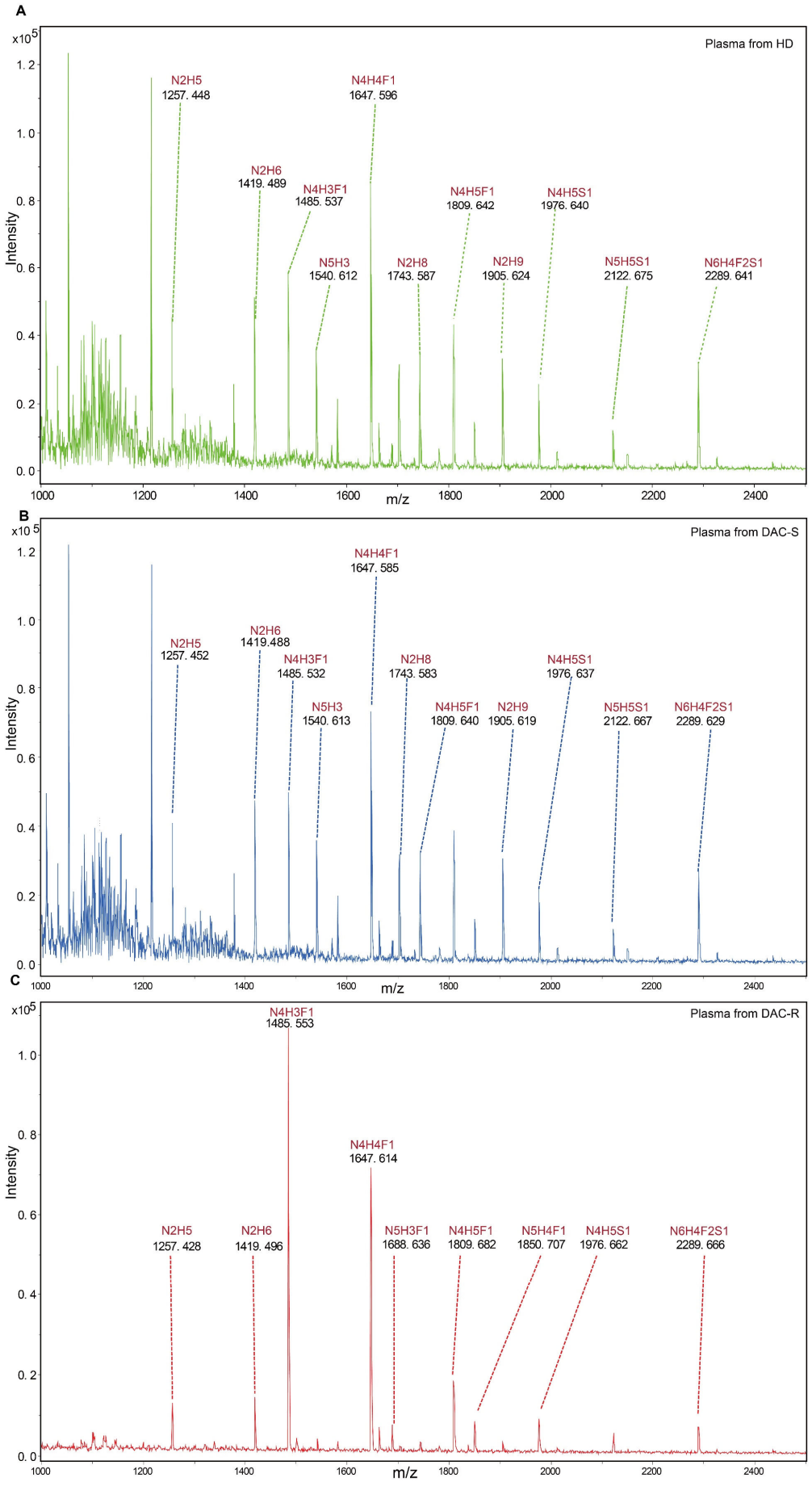
A
Plasma from HD
x10 5
Intensity
m/z
N2H5 1257. 448
N4H4F1 1647. 596
N2H6 1419. 489
N4H3F1 1485. 537
N4H5F1 1809. 642
N4H5S1 1976. 640
N5H3 1540. 612
N2H8 1743. 587
N2H9 1905. 624
N5H5S1 2122. 675
N6H4F2S1 2289. 641
B
Plasma from DAC-S
N4H4F1 1647. 585
N2H5 1257. 452
N2H6 1419.488
N4H3F1 1485. 532
N2H8 1743. 583
N4H5S1 1976. 637
N5H3 1540. 613
N4H5F1 1809. 640
N2H9 1905. 619
N5H5S1 2122. 667
N6H4F2S1 2289. 629
C
Plasma from DAC-R
N4H3F1 1485. 553
N4H4F1 1647. 614
N2H5 1257. 428
N2H6 1419. 496
N5H3F1 1688. 636
N4H5F1 1809. 682
N5H4F1 1850. 707
N4H5S1 1976. 662
N6H4F2S1 2289. 666

Fig. S4. (A) Relative abundance of fucosylated and non-fucosylated N-glycans in plasma from healthy donors (HD), decitabine-sensitive (DAC-S), and decitabine-refractory (DAC-R) patients. (B) Relative intensity of individual fucosylated N-glycan compositions in plasma from HD, DAC-S, and DAC-R patients. (C) Fold change of individual fucosylated N-glycan compositions normalized to the HD group. (D) Representative MALDI-TOF/TOF–MS spectra of N-glycans in sEVs from KG1a and KG1a-DAC cells. Peaks with signal-to-noise ratio >5 were included for relative intensity analysis. Glycan compositions are annotated using the H/N/F/S nomenclature (H, hexose; N, N-acetylglucosamine; F, fucose; S, sialic acid). (E) Relative intensity of individual N-glycan compositions in sEVs from KG1a and KG1a-DAC cells. (F) AAL-reactive signal in plasma from HD, DAC-S, and DAC-R samples determined by ELISA. (G) Immunoblot analysis of FUT4 expression in KG1a and KG1a-DAC cells. (H) Le^X levels in KG1a-DAC cells with or without PNGase F treatment. (I) Le^X levels in plasma-derived sEVs from HD, DAC-S, and DAC-R samples. (J) Le^X levels in KG1a and KG1a-DAC cells assessed by flow cytometry (representative histograms and mean fluorescence intensity quantification). Data are mean ± SEM; experiments were repeated three times with similar results. ns, not significant; *P<0.05; **P<0.01; ***P<0.001.

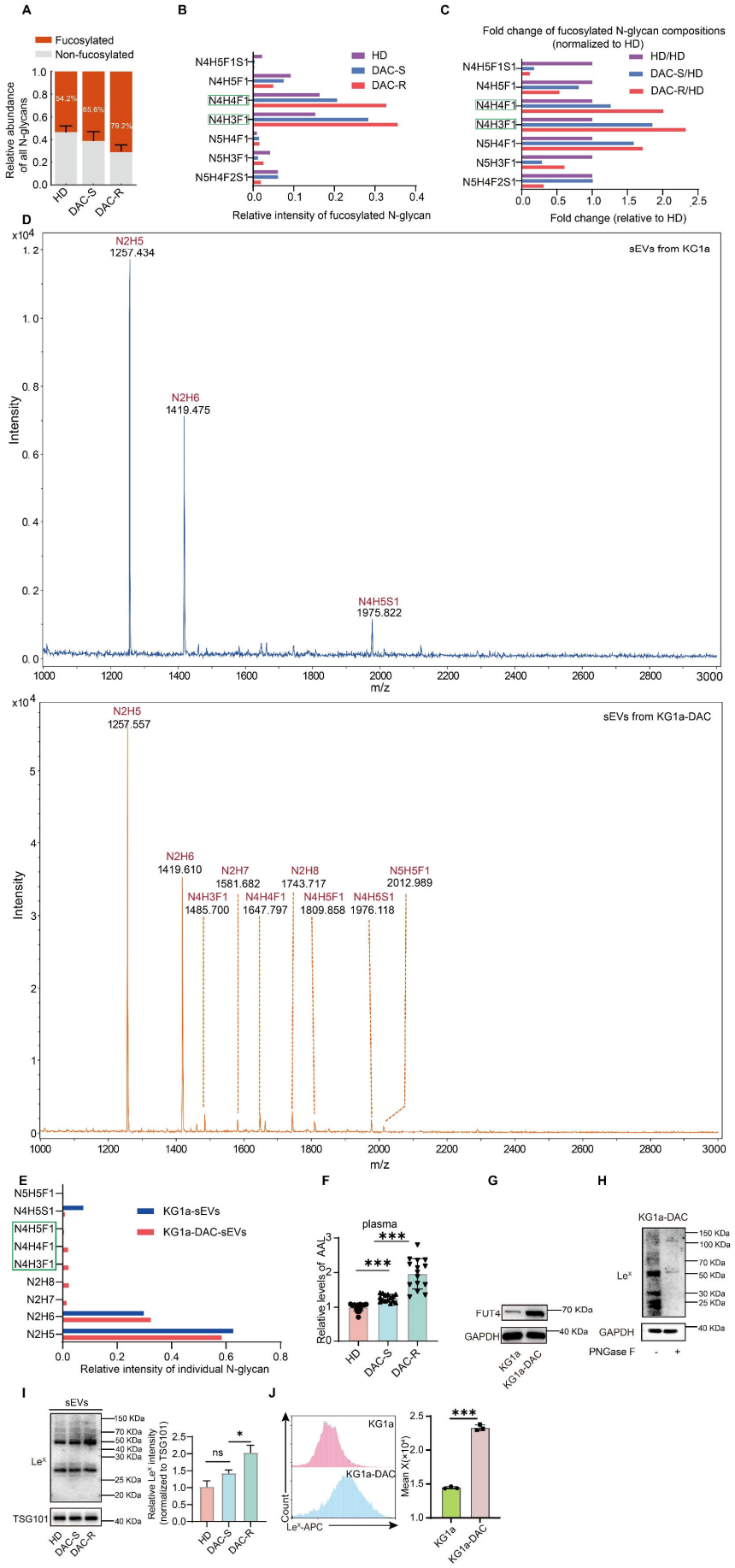
A
Fucosylated
Non-fucosylated
Relative abundance of all N-glycans
54.2%
65.6%
79.2%
HD
DAC-S
DAC-R
B
HD
DAC-S
DAC-R
N4H5F1S1
N4H5F1
N4H4F1
N4H3F1
N5H4F1
N5H3F1
N5H4F2S1
Relative intensity of fucosylated N-glycan
C
Fold change of fucosylated N-glycan compositions (normalized to HD)
HD/HD
DAC-S/HD
DAC-R/HD
Fold change (relative to HD)
D
sEVs from KG1a
N2H5
1257.434
N2H6
1419.475
N4H5S1
1975.822
Intensity
m/z
sEVs from KG1a-DAC
N2H5
1257.557
N2H6
1419.610
N2H7
1581.682
N2H8
1743.717
N5H5F1
2012.989
N4H3F1
1485.700
N4H4F1
1647.797
N4H5F1
1809.858
N4H5S1
1976.118
E
KG1a-sEVs
KG1a-DAC-sEVs
Relative intensity of individual N-glycan
F
plasma
Relative levels of AAL
HD
DAC-S
DAC-R
G
FUT4
70 KDa
GAPDH
40 KDa
KG1a
KG1a-DAC
H
KG1a-DAC
Le^x
GAPDH
PNGase F
I
sEVs
Le^x
TSG101
HD
DAC-S
DAC-R
Relative Le^x intensity (normalized to TSG101)
ns
J
KG1a
KG1a-DAC
Count
Le^x-APC
Mean X(×10^4)

Fig. S5. (A) Immunoblot analysis of tight junction–related proteins in human umbilical vein endothelial cells (HUVECs) after exposure to conditioned medium (CM) from KG1a or KG1a-FUT4. (B, C) HUVEC permeability to rhodamine B–labeled dextran (OD590) and transendothelial migration (relative invaded $CD45^+$ cell ratio) after exposure to the indicated CM. (D) Angiogenesis metrics (junction count and total branching length) in HUVECs treated with the indicated CM. (E, F) FUT4 expression and Lewis X (Le^X) levels in KG1a-DAC-shFUT4 cells and their derived small extracellular vesicles (sEVs). (G, H) Immunoblot analysis of tight junction–related proteins in HUVECs after exposure to CM or sEVs from KG1a-DAC or KG1a-DAC-shFUT4. (I, J) HUVEC permeability (OD590) and transendothelial migration (relative invaded $CD45^+$ cell ratio) after exposure to the indicated sEVs or CM. (K, L) Angiogenesis metrics (junction count and total branching length) in HUVECs treated with the indicated CM or sEVs. (M) Immunoblot analysis of tight junction–related proteins in HUVECs treated with OptiPrep-purified sEVs from KG1a, KG1a-DAC, KG1a-FUT4, and KG1a-DAC-shFUT4 cells. (N) Quantification of human $CD45^+$ cells in blood, bone marrow, and spleen in mice preconditioned with HD-sEVs or KG1a-sEVs. Data are mean ± SEM; experiments were repeated three times with similar results. *P<0.05; **P<0.01; ***P<0.001.

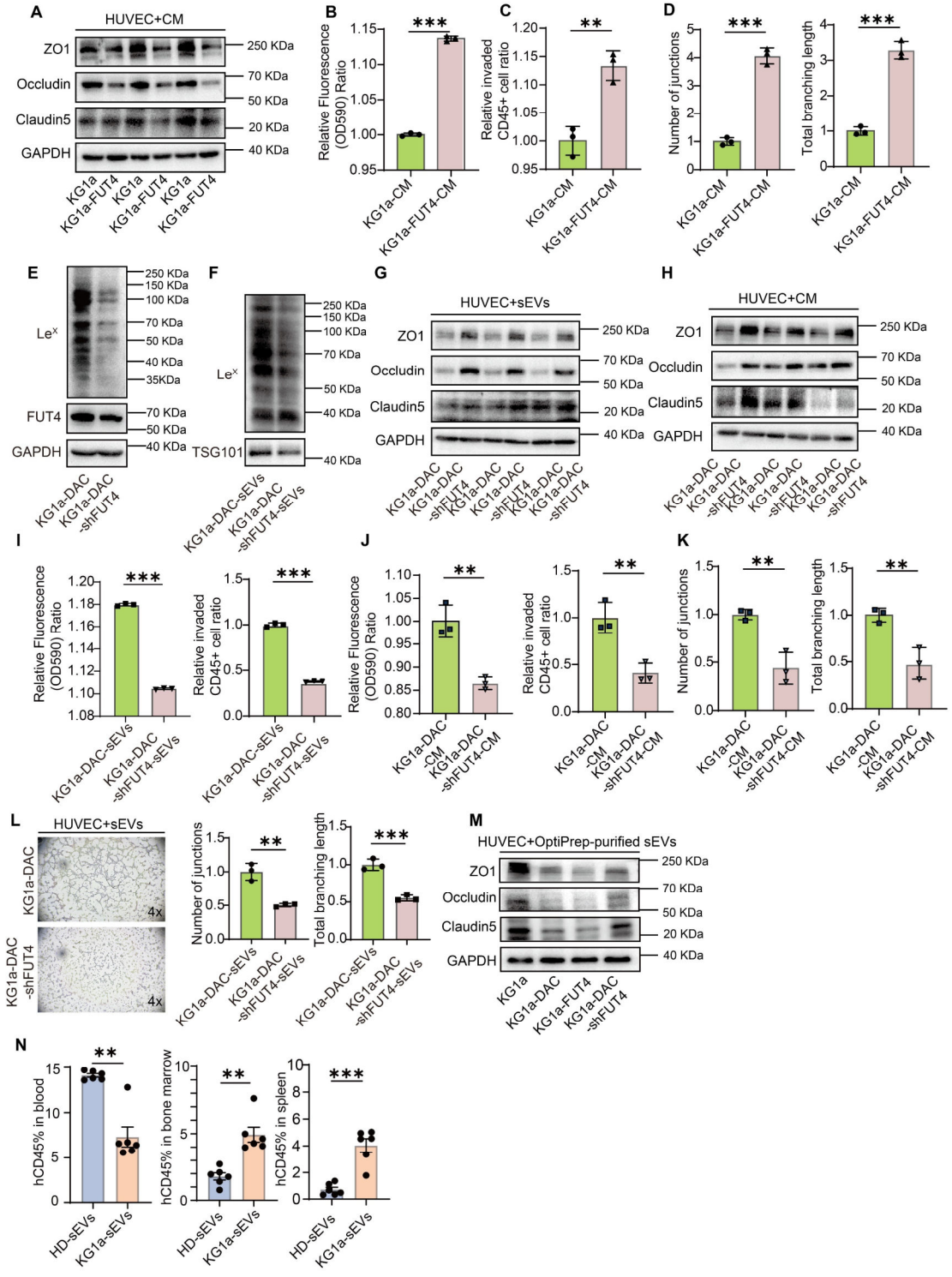

Fig. S6. (A) Expression of FUT4 and TWIST1 at mRNA levels in KG1a and KG1a-TWIST1 cells. (B&C) Expression of FUT4, TWIST1 at protein and mRNA levels and the levels of Le^X in SKM1 and SKM1-shTWIST1 cells. (D) Tight junction related-proteins and (E&F) permeability in HUVECs after treated with CM from SKM1 and

SKM1-shTWIST1. (G) Angiogenesis metrics in HUVECs treated with CM from SKM1 and SKM1-shTWIST1. (H) TWIST1 binding to E-box motifs within the 0–2000 bp region of the FUT4 promoter. (I) TWIST1 binding sites on wild-type (WT) and mutant sequences of E-box motif 1, 2 and 7 of FUT4 promoter. Data are mean ± SEM; experiments were repeated three times with similar results. *P<0.05; **P<0.01; ***P<0.001.

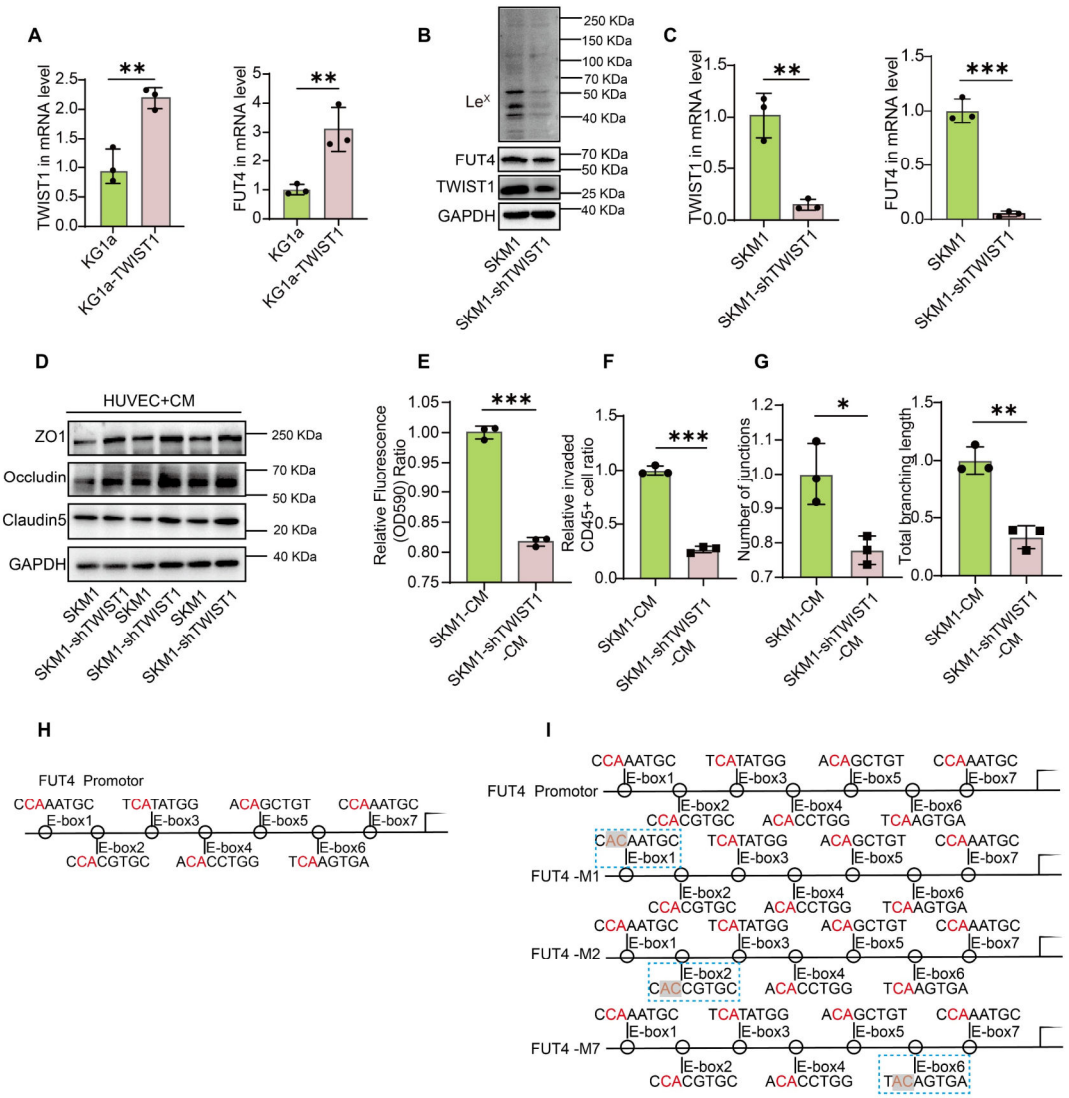

Fig. S7. (A) Immunoblot analysis of density gradient fractions showing sEV markers and ICAM3 in sEVs isolated from KG1a cells. (B) Expression of ICAM3 and Le^X in OptiPrep-purified sEVs derived from KG1a, KG1a-DAC, KG1a-FUT4, and KG1a-DAC-

shFUT4 cells. (C) Expression of ICAM3 in ultracentrifugation-isolated sEVs from the indicated cells. (D) ICAM3 stability in KG1a and KG1a-FUT4 cells after cycloheximide (CHX) treatment for the indicated times. (E) ICAM3 expression in KG1a cells treated with CHX in the presence or absence of MG132 or chloroquine (Chlo) for 8 h. (F–J) Immunoblot analysis of NF-κB signaling components (p65, p-p65, IκBα, p-IκBα) and tight junction–related proteins in HUVECs treated with BAY-11-7082 (F, G), phorbol 12-myristate 13-acetate (PMA) (H, I), or sEVs from the indicated cells (J).

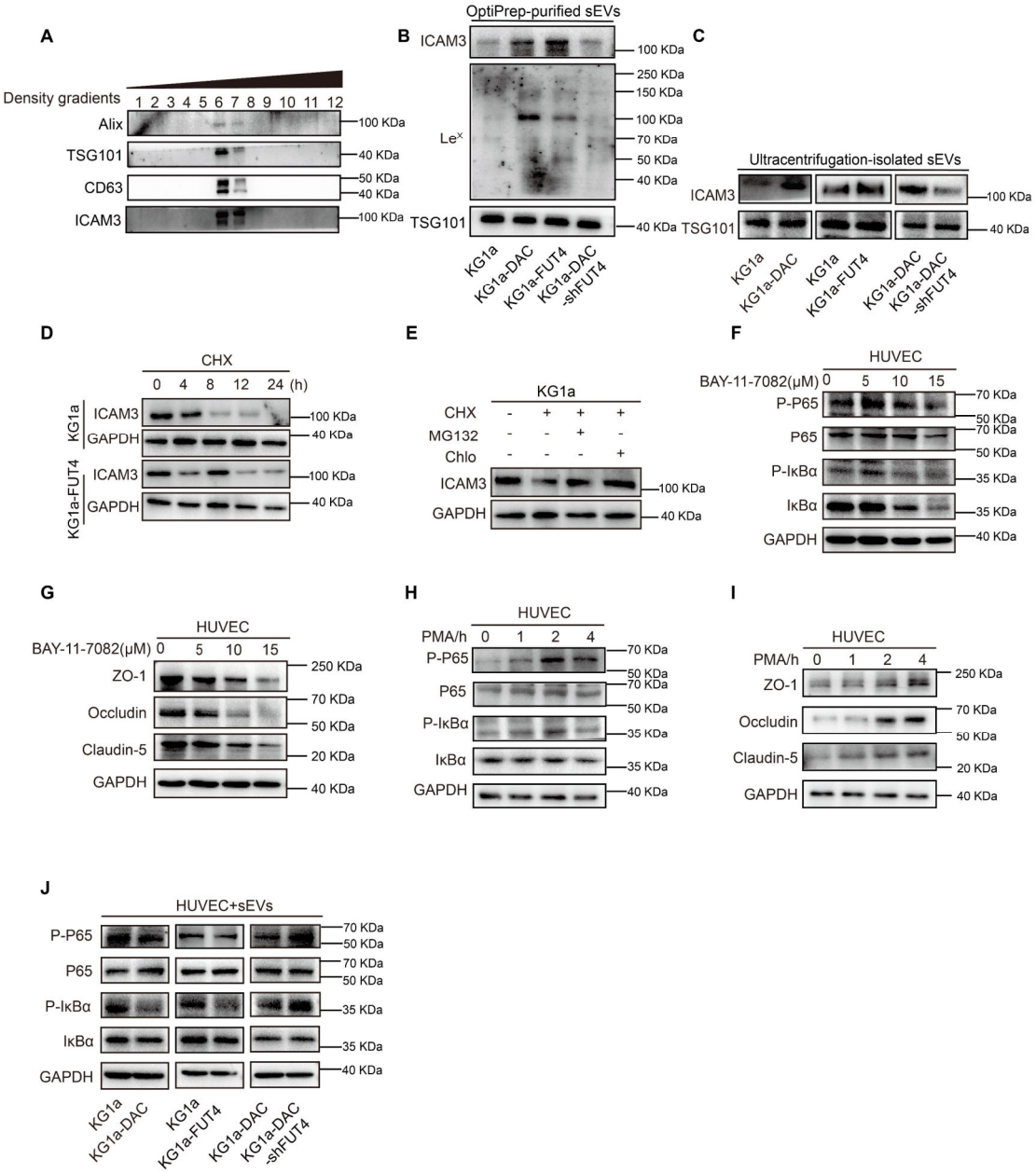

Fig. S8. (A) Expression of tight junction–related proteins and NF-κB signaling components (p65, p-p65, IκBα, p-IκBα) in HUVECs cocultured with KG1a-DAC cells in the presence or absence of anti-human ICAM3 antibody (a-ICAM3). (B, C) HUVEC permeability and leukemic cell transendothelial migration, and (D) angiogenesis metrics of HUVECs cocultured with indicated cells with or without a-ICAM3. (E) Expression of tight junction–related proteins and NF-κB signaling components (p65, p-p65, IκBα, p-IκBα) in HUVECs cocultured with KG1a-DAC-shFUT4 cells with or without

recombinant ICAM3 (rICAM3). (F, G) HUVEC permeability and leukemic cell transendothelial migration, and (H) angiogenesis metrics of HUVECs cocultured with indicated cells with or without rICAM3. (I) Immunoblot analysis of ICAM3 and NF-κB signaling components (p65, p-p65, IκBα, p-IκBα) in HUVEC and HUVEC-ICAM3. (J) Immunoblot analysis of tight junction–related proteins and ICAM3 in HUVEC and HUVEC-ICAM3. (K, L) HUVEC permeability and leukemic cell transendothelial migration in HUVEC and HUVEC-ICAM3. (M) Angiogenesis metrics, including junction count and total branching length, were quantified in HUVEC and HUVEC-ICAM3. Data are mean ± SEM; experiments were repeated three times with similar results. *P<0.05; **P<0.01; ***P<0.001.

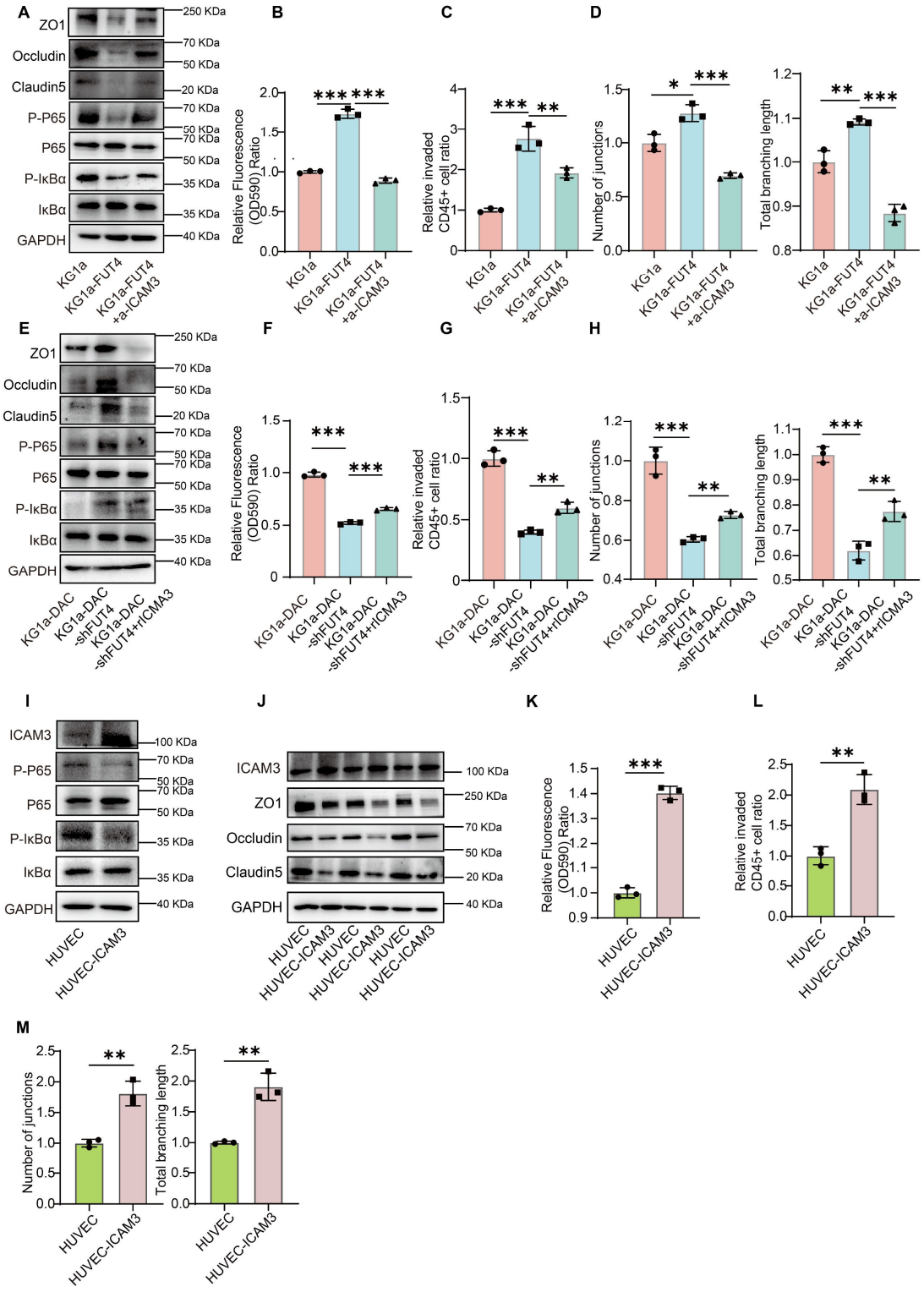

Supplementary tables

Tab. S1 Patients list

Diagnosis	Age	Gender	Cytogenetics	BM Cellularity	Marrow Blast Count	DAC Response

AML	69	M	Normal	Hypercellular	41%	R
MDS-EB2	54	M	Normal	Normal	16.80%	R
AML	73	F	Normal	Hypercellular	43%	R
AML	48	M	Normal	Hypercellular	45%	R
AML	31	F	Normal	Hypercellular	53%	R
AML	48	F	Normal	Hypercellular	61%	R
MDS-EB1	35	M	Normal	Hypercellular	12%	R
MDS-EB2	31	M	Normal	Hypercellular	14%	R
MDS-EB2	56	M	Normal	Hypercellular	13%	R
AML	77	F	Normal	Hypercellular	24%	R
AML	64	M	Normal	Normal	35%	R
MDS-EB2	72	F	Normal	Normal	17%	R
AML	53	F	Normal	Hypercellular	27%	R
AML	62	F	t(8;21)(q22;q22)	Normal	30%	R
MDS-EB2	65	M	Normal	Hypercellular	15%	R
MDS-EB1	75	F	Normal	Hypercellular	12%	R
MDS-EB2	76	F	Normal	Hypercellular	14%	R
AML	67	F	Normal	Hypercellular	25%	R
AML	70	M	Normal	Hypercellular	25%	R
AML	78	F	Normal	Normal	40%	S
MDS-MLD	65	M	Normal	Normal	6.50%	S
MDS-EB1	62	M	Normal	Normal	8%	S
AML	48	M	t(8;21)(q22;q22)	Hypercellular	23.50%	S
AML	58	M	Normal	Hypercellular	29%	S
MDS-EB2	66	F	Complex karyotype	Normal	23%	S
AML	43	F	t(8;21)(q22;q22), +8	Hypercellular	29%	S
AML	58	F	Normal	Normal	32%	S
AML	68	M	Normal	Normal	22%	S
MDS-EB1	44	F	Normal	Normal	5%	S
MDS-EB1	61	F	Normal	Hypercellular	9%	S
MDS-EB2	75	F	Complex karyotype	Hypercellular	14%	S
AML	30	M	Normal	Hypercellular	30%	S
AML	79	M	Normal	Normal	45%	S
AML	32	F	t(8;21)(q22;q22)	Hypercellular	36%	S
AML	68	F	Normal	Hypercellular	28%	S
MDS-EB2	76	M	Complex karyotype	Normal	25%	S

MDS-EB1	74	M	Normal	Normal	8%	S
HD	45	F				
HD	36	F				
HD	35	M				
HD	58	F				
HD	27	M				
HD	36	F				
HD	45	F				
HD	28	F				
HD	61	F				
HD	23	F				
HD	57	M				
HD	60	M				
HD	61	M				
HD	49	M				
HD	28	M				
HD	70	F				
HD	61	F				
HD	69	M				
HD	48	M				

Tab. S2 Primer list for chip

Primers	Sequences
FUT4-E-box-1-F	CGAGGTAAGAGGGCACAAAGAAAAT
FUT4-E-box-1-R	AGGCATTTGGGAAATATTACCCTGC
FUT4-E-box-2-F	GCCACGTGCCAGACACAATGTT
FUT4-E-box-2-R	AGGTGTTCTGGCTAGGCCCAT
FUT4-E-box-3-F	TCTCGATCTCCTGACCT
FUT4-E-box-3-R	ATTTGCGTTAGCCATATG
FUT4-E-box-4-F	AACACCTGGCAGGATTG
FUT4-E-box-4-R	AGCTGTGCATCAGTGGA
FUT4-E-box-5-F	AGTATCAGTGGGACTCCACT

FUT4-E-box-5-R	TCTGGGTGTTCGCTTTG
FUT4-E-box-6-F	TCTCAAGTGACTGTAGACGT
FUT4-E-box-6-R	ATTCTAGCACCCAAGTTAAGG
FUT4-E-box-7-F	GTTCTCTATCCTTTACTGGGCT
FUT4-E-box-7-R	AGACGGTCGAATTGTGGAG

Tab. S3 Primer list for dual luciferase reporter assay

Primers	Sequences
FUT4-F	AGATCGCCGTGTAATTCTAGATGCGAAGTCACGACTGGTTTC
FUT4-R	AGGGCATCGGTCGACGGATCCGGAGGATAGCGTCGGCTTCC
FUT4-E-BOX-1F'	GTAATATTTCCACAATGCCTACCGGCCACGT
FUT4-E-BOX-1R'	CGGTAGGCATTGTGGAAATATTACCCTGCTTGATTGC
FUT4-E-BOX-2F'	TACCGGCACCGTGCCAGACACAAT
FUT4-E-BOX-2R'	ATTGTGTCTGGCACGGTGCCGGTAGGCATTTGGGA
FUT4-E-BOX-7F'	CACACAATGCAGAGACTCTGAAGGCCA
FUT4-E-BOX-7R'	CCTTCAGAGTCTCTGCATTGTGTGAAGAACTTAAG

Tab. S4 see Excel File

Identified N-glycans in plasma from HD, DAC-S, and DAC-R patients and in sEVs from KG1a and KG1a-DAC cells, as determined by MALDI-TOF/TOF-MS.

Supplemental Reference

1. Lei L, Wang Y, Liu R, et al. Transfer of miR-4755-5p through extracellular vesicles and particles induces decitabine resistance in recipient cells by targeting CDKN2B. Mol Carcinog. 2023;62(6):743-753.

2. Sung BH, Ketova T, Hoshino D, Zijlstra A, Weaver AM. Directional cell movement through tissues is controlled by exosome secretion. Nat Commun. 2015;6:7164.

3. Beer LA, Liu P, Ky B, Barnhart KT, Speicher DW. Efficient Quantitative Comparisons of Plasma Proteomes Using Label-Free Analysis with MaxQuant. Methods Mol Biol. 2017;1619:339-352.

4. Cao L, Zhou Y, Li X, Lin S, Tan Z, Guan F. Integrating transcriptomics, proteomics, glycomics and glycoproteomics to characterize paclitaxel resistance in breast cancer cells. J Proteomics. 2021;243:104266.

5. Ceroni A, Maass K, Geyer H, Geyer R, Dell A, Haslam SM. GlycoWorkbench: a tool for the computer-assisted annotation of mass spectra of glycans. J Proteome Res. 2008;7(4):1650-1659.

6. Wang R, Liu Y, Wang C, et al. Comparison of the methods for profiling N-glycans-hepatocellular carcinoma serum glycomics study. RSC Adv. 2018;8(46):26116-26123.

7. Ramachandran P, Xu G, Huang HH, et al. Serum Glycoprotein Markers in Nonalcoholic Steatohepatitis and Hepatocellular Carcinoma. J Proteome Res. 2022;21(4):1083-1094.

8. Tsai TH, Wang M, Di Poto C, et al. LC-MS profiling of N-Glycans derived from human serum samples for biomarker discovery in hepatocellular carcinoma. J Proteome Res. 2014;13(11):4859-4868.

9. Li H, Wang Y, Feng S, et al. Reciprocal regulation of TWIST1 and OGT determines the decitabine efficacy in MDS/AML. Cell Commun Signal. 2023;21(1):255.

10. Li H, Wang Y, Pang X, et al. Elevated TWIST1 expression in myelodysplastic syndromes/acute myeloid leukemia reduces efficacy of hypomethylating therapy with decitabine. Haematologica. 2020;105(10):e502.

11. Tan Z, Cao L, Wu Y, et al. Bisecting GlcNAc modification diminishes the pro-metastatic functions of small extracellular vesicles from breast cancer cells. J Extracell Vesicles. 2020;10(1):e12005.